PHYS4080 Content Notes

Ryan White
s4499039

Semester 2, 2023

1 Week 1

Ch 8.7 – Cosmological Parameters

8.7.1 – The Standard Cosmological Model from CMB Measurements

The base model. According to the model of inflation in the early universe, our Universe is expected to be spatially flat. Such a model is described by a minimum of six parameters. Two of them characterise the initial density fluctuations (namely an amplitude A and the power-law slope n_s). As a third parameters, the post-reionisation scattering optical depth τ needs to be chosen. The remaining three parameters describe the energy contents and scale of the universe. The three typically used are $\omega_b \equiv \Omega_b h^2$ (subscript b for baryonic matter), $\omega_c \equiv \Omega_c h^2$ (where $\Omega_c = \Omega_m - \Omega_b$ is the density parameter of cold dark matter), and Ω_Λ.

8.7.2 – Consistency and Discrepancies with Other Measurements

Baryonic Acoustic Oscillations. The results from BAO studies of galaxy distributions is perfectly compatible with the cosmological model parameters as determined by WMAP. Furthermore, one can also compare the observed power spectrum of galaxies with the predictions from the standard model (using the best-fit parameters). The agreement again is excellent on large scales; on smaller scales, slight discrepancies appear which mostly likely are due to non-linear effects in structure formation, and thus also in the clustering of galaxies.

8.7.3 – Extensions of the Standard Model

Although the standard model, defined by the six basic parameters mentioned earlier, provides an excellent fit to the CMB data – temperature fluctuation power spectrum out to $l = 2500$, low-l polarisation fluctuations, and the CMB lensing effects – it is worth generalising this model by considering extensions in various ways.

Curvature. The standard model assumes spatial flatness. The CMB data, together with the lensing information and BAO studies, gives a spatial flatness estimate of $(\Omega_m + \Omega_\Lambda - 1) = 0.10^{+0.65}_{-0.62}\%$. Hence, there is very little room for generalising the model away from flatness.

Number of Neutrino Families and their Masses. The standard model assumes that there are three families of neutrinos, and that they are essentially massless. Relaxing one or both of these assumptions, we can see whether the CMB data preferences a non-standard picture of the neutrinos. If the sum of the neutrino masses is significantly larger than the minimum mass required from neutrino oscillations, then they would contribute to the current matter density in the Universe in the form of hot dark matter, and thus affect the shape of the power spectrum. If the number of neutrino families is larger than three, there would be a larger radiation component in the early universe, changing the expansion law and the epoch of matter-radiation equality. All of this affects the CMB fluctuations.
The CMB and BAO data together yield $\sum m_\nu < 0.28$ eV, and $N_{\rm eff} = 3.32^{+0.54}_{-0.52}$. This result confirms our picture of particle physics, according to which there are three families of leptons, and thus three kinds of neutrinos.

Big Bang Nucleosynthesis. The standard model assumes that the helium abundance following the first few minutes after the Big Bang is given by the theory of nucleosynthesis, and is therefore a function of $\omega_b \equiv \Omega_b h^2$. This helium abundance then determines the evolution of the number density of free electrons before recombination, since helium recombines earlier than hydrogen because of its higher ionization potential. The value of ω_b, as determined from CMB anisotropies, is in excellent agreement with the results obtained from the observed abundance of helium and deuterium in the Universe. Leaving the helium abundance as a free parameter and using the CMB data to directly predict it, one obtains a result in excellent agreement to BBN, and hence very strongly rules out any exotic model that wants to explain the current helium contents of the Universe solely by nuclear fusion in stars.

8.7.4 – Cosmic Harmony

Hubble Constant. H_0 was determined by means of the distance ladder, particularly using Cepheids. All of the methods of measuring H_0 suggest that the Hubble constant is within 5% of 71 km s^{-1}Mpc^{-1}, or $h \approx 1/\sqrt{2}$.
Contribution of Baryons to the Total Matter Density. The ratio Ω_b/Ω_m is determined from the baryon fraction in clusters of galaxies, from redshift surveys of galaxies, and from the CMB fluctuations, all yielding $\Omega_b/\Omega_m \approx 0.15$.

Ch 8.8 – Dark Energy: Cosmological Constant, or Something Else?

The cosmological constant and Einstein's field equation. Einstein's field equation of general relativity can be expressed as

$$G = T \tag{8.43}$$

where G (called the Einstein tensor) describes the curvature of spacetime and thus the effects of gravity, whereas T (the so-called energy-momentum tensor) contains information about the matter and energy density. As it stands, equation (8.43) does not allow a static cosmos, and so Einstein modified his equation to include the cosmological constant which then reads

$$G - \Lambda = T \tag{8.44}$$

With this modification, one can construct a static model. A modern interpretation of the cosmological constant is obtained by slightly rewriting (8.44) as

$$G = T + \Lambda \tag{8.45}$$

where now the Λ-term is seen as a contribution to the source of the gravitational field; it has the same structure as one would get from a constant, uniform vacuum energy density. The difference of the interpretation is that instead of Λ

being a modification of the laws of gravity, it adds a new energy component as a source of gravity.

Time-varying dark energy. There are ideas that the value of the vacuum energy density is actually not a constant in time, but that it may vary. In that case, the dark energy density would be a function of cosmic epoch, $\rho_{\rm DE}(a)$. The question of whether dark energy is compatible with a cosmological constant, or has more complicated properties, is a very interesting one: if it were not constant in time, then it must have a more dynamical origin which would clearly argue against it being another fundamental constant of nature. One therefore considers it as a possible variant of the cosmological constant an equation-of-state of dark energy of the form

$$P_{\rm DE} = w\rho_{\rm DE}c^2 \tag{8.46}$$

where $w = -1$ corresponds to the cosmological constant. In order for this component to potentially lead to an accelerated expansion, the second Friedmann equation requires $w < -1/3$.
In fact, the equation-of-state parameter w does not need to be a constant, and can vary with cosmic epoch. Can one observationally distinguish between the case $w = -1$ for a cosmological constant (or a vacuum energy density that is indistinguishable from a cosmological constant) and the more interesting, dynamical case of $w \neq -1$?. The first major impact of $w \neq -1$ on cosmology would be a change of the expansion rate $H(a)$ of the universe. Second, the growth rate of structure would be affected for a dynamical w.

Lecture 1

Unit Conversion. Most often, cross sections are given in units of GeV^{-2} or $\mathrm{cm}^3\mathrm{s}^{-1}$. To convert between them, we employ

$$\frac{\sigma v}{\mathrm{GeV}^{-2}} = \frac{\sigma v}{\mathrm{cm}^3\mathrm{s}^{-1}} \times \frac{1}{1.17 \times 10^{-17}}$$

Lecture 2

Dark matter is the only way to consistently explain rotation curves of galaxies (and the velocity dispersions in elliptical galaxies), the magnitude of gravitational lensing, and cosmological data (which says that $\Omega_{\rm matter} \simeq 0.27$, where big bang nucleosynthesis says $\Omega_{\rm baryonic} \approx 0.04$ and hence $\Omega_{\text{non-baryonic}} \sim 5\Omega_{\rm baryons}$).

What we know about dark matter

Dark matter as we know it must be massive (because of its gravitational interaction), unable to interact via electromagnetism (and hence it's dark), non-baryonic (lest BBN would have accounted for it), cold-ish (in order to allow large scale structure formation), stable on cosmological timescales (otherwise it would have decayed by now), and produced in the right relic abundance in the early universe.

Primordial black holes, massive compact halo objects, and standard model neutrinos all come with their own problems as descriptors of dark matter (MACHOs would be baryonic, and SM neutrinos are too warm). Hence, we turn mainly to Weakly Interacting Massive Particles and axions to describe it.
We don't know what mass these particles are (the possible mass range spans 90 orders of magnitude), their interactions, coupling, etc although many of these properties have been constrained by observations (or lack thereof).

Detection Strategies

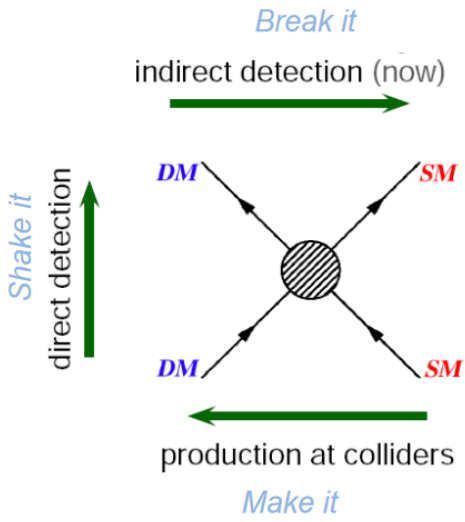

Direct detection – nuclear collisions and recoils
Indirect detection – annihilations producing SM particles (maybe even from DM that has sunk to the center of stars and annihilates into neutrinos)
Direct production – missing E_T or otherwise in LHC or future colliders.

WIMPs

WIMPs as we hypothesise them are dark (no electromagnetic interactions), cold (as they're very massive [$\sim$ 10 GeV to $\sim$ 10 TeV]), non-baryonic and stable (and so no problems with BBN or the CMB). The weak force interaction implies some scattering with atomic nuclei, and many WIMPs are Majorana particles (i.e. their own antiparticle) and so their self-annihilation provides a detection channel.

Dark Matter Density Profiles

Rotation curves place good constraints on the density profiles of dark matter within galaxies and clusters, and essentially tell us that dark matter is gravitationally bound, more or less frictionless, and comprise dark matter halos within galaxies. N-body simulations of dark matter halo formation suggesta universal Navarro-Frenk-White profile

$$\rho(r) = \frac{\delta_c \rho_c}{\frac{r}{r_s}(1+\frac{r}{r_s})^2}$$

or Einasto profile

$$\rho(r) = \rho_s \exp\left(-2n\left[(r/r_s)^{1/n} - 1\right]\right)$$

These profiles may be steepened in the innermost regions by adiabatic contraction or softened by baryonic effects. For low mass galaxies in particular, there is some discrepancy between simulations and the data with sims implying a "cusp" (higher density DM) at small radius, but data implies a "core" (flattening profile) at low radius.

The galactic dark matter halo is *isothermal* to a first approximation and so a WIMP wind is predicted as the solar system moves through the randomly oriented DM particle motion.

Thermal Production

A particle with a larger interaction cross section, $\langle \sigma v \rangle$, can withstand more universe expansion before its abundance 'freezes out' (i.e. its abundance stabilises).

2 Week 2

Lecture 3

Direct Detection

How would we know? To discern a signal from noise, we'd need a detection at several different detectors. Additionally, we expect some directional dependence and yearly modulation in a signal due to a WIMP "wind". The Earth + Sun velocity changes throughout the year, and the laboratory velocity changes throughout the day, and so as the Solar system moves through the Milky Way on its orbit, we should expect some WIMP wind as we move through the essentially randomly-moving WIMP particles. From the rate of Earth's orbital speed compared to the Suns orbital speed, and the plane of Earths orbit, we expect a 5% modulation in event rate and more if the cross-section is velocity dependent.

DM detectors are far underground to reduce noise from cosmic rays and particles.
Detection methods. Ionisation, scintillation (fluorescence with a quick recovery in a transparent medium), and vibration (phonons).

Lecture 4

Indirect Detection

Annihilation into photons is nice, since they usually travel straight and so we can look back to their sources. We have 3 main gamma-ray channels (figure below): monochromatic lines, internal bremsstrahlung, and continuum from a secondary decay product.
We want to look for targets with lots of DM, and few other astrophysical processes that produce gamma rays. Likely targets are dwarf galaxies (low γ background, but low statistics), the galactic center (large signal but large γ background), the galactic halo (moderate signal and background), clusters/extragalactic diffuse (large modelling uncertainties, low signal and low background), and dark clumps (low statistics and low background).

3 Week 3

4 Week 4

Ch 7.5 – Non-Linear Structure Evolution

7.5.1 – Model of Spherical Collapse

Assumptions. We consider a spherical region in an expanding universe, with its density $\rho(t)$ enhanced compared to the mean cosmic density $\overline{\rho}(t)$,

$$\rho(t) = [1 + \delta(t)]\overline{\rho}(t) \tag{7.46}$$

For reasons of simplicity we assume that the density within the sphere is homogeneous although, as we'll later see, this is not really a restriction. The density perturbation is assumed to be small for small t so that it will grow linearly at first, $\delta(t) \propto D_+(t)$, as long as $\delta \ll 1$. If we consider a time t_i which is sufficiently early such that $\delta(t_i) \ll 1$, then according to the definition of the growth factor D_+, $\delta(t_i) = \delta_0 D_+(t_i)$, where

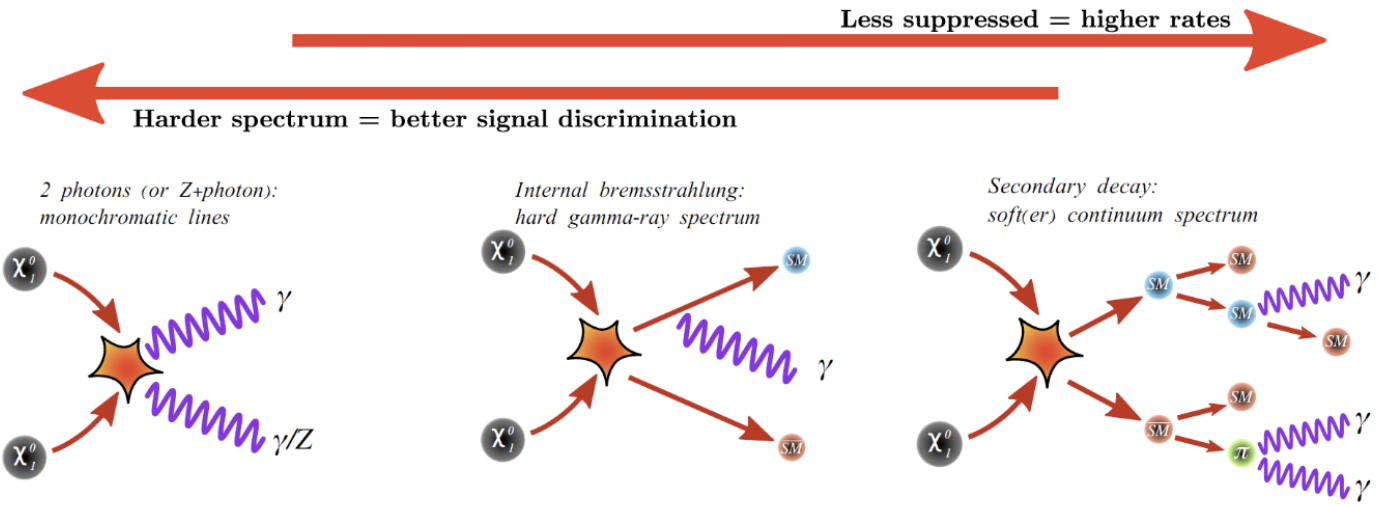

δ_0 is the density contrast linearly extrapolated to the present day. It should be mentioned once again that $\delta_0 \neq \delta(t_0)$, because the latter is in general affected by the non-linear evolution.
Let R be the initial *comoving* radius of the overdense sphere; as long as $\delta \ll 1$, the comoving radius will change only marginally. The mass within the sphere is

$$M = \frac{4\pi}{3} R^3 \rho_0 (1 + \delta_i) \approx \frac{4\pi}{3} R^3 \rho_0 \tag{7.47}$$

Evolution. Due to the enhanced gravitational force, the sphere will expand slightly more slowly than the universe as a whole, which will lead to an increase in its density contrast. This then decelerates the expansion rate (relative to the cosmic rate) even further. If the initial mass density within the sphere is sufficiently large, the expansion of the sphere will come to a halt, i.e., its proper radius $R_{\rm phys}(t)$ will reach a maximum; after this, the sphere will recollapse. If $t_{\rm max}$ is the time of maximum expansion, then the sphere will, theoretically, collapse to a single point at time $t_{\rm coll} = 2t_{\rm max}$. This relation follows from the time reversal symmetry of the equation of motion.

Special case: Einstein-de Sitter model. In the special case of $\Omega_m = 1$, $\Omega_\Lambda = 0$, the Friedmann equations can be solved to yield a recollapse time at the present epoch corresponding to an overdensity of

$$\delta_c \simeq 1.69 \tag{7.48}$$

More generally, for a recollapse before redshift z, one needs $\delta_0 \geq \delta_c(1+z)$ (although the critical overdensity is cosmology dependent).

Violent Relaxation and Virial Equilibrium. Of course, the sphere will not really collapse to a single point. In reality, small scale density and gravitational fluctuation will exist within such a sphere which lead to derivations in the particles' tracks from perfectly radial orbits. The particles will scatter on these fluctuations in the gravitational field and will virialize; this process occurs on short time-scales – roughly the dynamical time-scale (i.e. the time it takes for particles to fully cross the sphere). In this case, the virialization is essentially complete at $t_{\rm coll}$. After that, the sphere will be in virial equilibrium and its average density will be $(1 + \delta_{\rm vir}) \sim 178$. A conclusion from this consideration is that a massive galaxy cluster with a virial radius of $1.5h^{-1}$Mpc must have formed from the collapse of a region that originally had a comoving radius larger by about an order of magnitude. Such a virialized mass concentration of dark matter is called a ***dark matter halo***.

7.5.2 – Number Density of Dark Matter Halos

The Mass Spectrum. We consider the number density of relaxed dark matter halos in the universe, $n(M, z)$, which is a function of mass M and redshift z.
We find that $n(M, z)$ is a decreasing function of halo mass. For large M, $n(M, z)$ decreases exponentially because sufficiently high peaks (of the initial mass function) become very rare for large distance scales. Therefore, *very* few clusters with $M \gtrsim 2 \times 10^{15} M_\odot$ exist today. At higher redshift, the cut-off in the abundance is at smaller masses, so that massive clusters are expected to be increasingly rare at higher z.

Hierarchical Structure Formation. The Press-Schechter model (i.e. the spherical collapse formation of DM halos) describes a very general property of structure formation in a CDM model, namely that low-mass structure (like galaxy-mass dark halos) format at early times, whereas large mass accumulations evolve only later. This is an example of a ***bottom-up scenario***, in which small structures that form early merge to form large structures.

Ch 7.6 – Properties of Dark Matter Halos

7.6.1 – Profile of Dark Matter Halos

Dark matter halos can be identified in mass distributions generated by numerical simulations. If we define a halo as a spherical region within which the average density is ~ 200 times the critical density at the respective redshift, the mass M of the halo is related to its (virial) radius r_{200} by

$$M = \frac{100 r_{200}^3 H^2(z)}{G} \tag{7.56}$$

so that each redshift, a unique relation exists between the halo mass and its radius. We can also define the virial velocity V_{200} of a halo as the circular velocity at the virial radius

$$V_{200}^2 = \frac{GM}{r_{200}} \tag{7.57}$$

We can combine the two above equations to express the halo mass and virial radius as a function of the virial velocity,

$$M = \frac{V_{200}^3}{10GH(z)}; \qquad r_{200} = \frac{V_{200}}{10H(z)} \tag{7.58}$$

Since the Hubble function $H(z)$ increases with redshift, the virial radius at fixed virial velocity decreases with redshift. We also see that r_{200} decreases with redshift at fixed halo mass. Hence, halos at a given mass (or given virial velocity) are more compact at higher redshift than they are today because the critical density was higher in the past.

The NFW Profile. The ***density profile*** of halos averaged over spherical shells seems to have a universal functional form described by

$$\rho(r) = \frac{\rho_s}{(r/r_s)(1 + r/r_s)^2} \tag{7.59}$$

where r_s specifies a characteristic radius, and $\rho_s = 4\rho(r_s)$ determines the amplitude of the density profile. For $r \ll r_s$ we find $\rho \propto r^{-1}$, whereas for $r \gg r_s$ the profile follows $\rho \propto r^{-3}$. Therefore, r_s is the radius at which the slope of the density profile changes. We define the ***concentration index*** as

$$c \equiv \frac{r_{200}}{r_s} \tag{7.61}$$

where the larger the value of c, the more strongly the mass is concentrated towards the inner regions. We can write the density profile amplitude factor as

$$\rho_s = \frac{200}{3}\rho_{\rm cr}(z)\frac{c^3}{\ln(1+c) - c/(1+c)}$$

where $\rho_{\rm cr}(z) = 3H^2(z)/(8\pi G)$ is the critical density at redshift z.

Comparison with Observations. A complication of modelling profiles with NFW (or other) profiles is that baryonic matter is present in the inner regions of galaxies (and clusters), thus contributing to the density, but also that these baryons have modified the density profile of dark matter halos in the course of cosmic evolution. Baryons are dissipative, they can cool, form a disk, and accrete inwards. Conversely, SNe can push gas to larger radii or even drive it out of the halo. The changes in the resulting density distribution of baryons by dissipative processes cause a change of the gravitational potential over time, to which dark matter also reacts. The dark matter profile in real galaxies is thus modified compare to pure dark matter simulations.

7.6.2 – The Shape and Spin of Halos

Halo Shapes. There is no reason for halos to have spherical symmetry. Approximating the surfaces of constant density in a halo by an ellipsoid of semi-axes $a_1 \leq a_2 \leq a_3$, the shape of a halo is characterised by the ratios $s = a_1/a_3$ and $q = a_2/a_3$. If $s = q < 1$, the ellipsoid is prolate, and a halo with $s < 1$ and $q = 1$ is oblate. If all three axes are different, the halo is triaxial.
Numerical simulations show that dark matter halos depend strongly on their formation time and merger history. If two halos of comparable mass collide and merge, the shape of the resulting halo will be strongly prolate. Halos that form early and experience no strong mergers tend to be more spherical.

Week 5

Ch 7.8 – The Substructure of Halos

Sub-halos of galaxies and clusters of galaxies. Numerical simulations of structure formation in the CDM model show that the mass density in halos is not smooth; instead, they reveal that halos contain numerous halos of much lower mass, so called sub-halos. For instance, a halo with the mass of a galaxy cluster contains hundreds or even thousands of halos with masses that are orders of magnitude lower. Similarly, a galaxy-mass halo will have sub-halos in the simulations. The presence of substructure over a wide range in mass is a direct consequence of hierarchical structure formation, in which objects of higher mass each contain smaller structure that have been formed earlier in the cosmic evolution.
Such simulations show that of order $\sim 10\%$ of the mass of halos is contained in sub-halos, with galaxy-mass halos having about $\sim 7\%$.

The spatial distribution of the sub-halos is less centrally concentrated than the total mass. The reason for this lies in the fact that the sub-halos whose orbits bring them deep into the potential well of the host halo are subject to strong tidal forces and get disrupted in the course of evolution. Simulations that include gas physics find that disruption becomes weaker if baryons are included – their dissipational nature leads to more compact (and thus more tightly bound) sub-halos which can resist tidal forces for longer.

The 'substructure' problem. The apparent deficit in the number of observed sub-halos within a galaxy-mass halo is considered to be a potential problem of CDM models. One possibility is that many of the sub-halos are extremely non-luminous and have just not yet been found. Indeed, the currently identified sub-halos (such as satellite galaxies) generally have a high velocity dispersion and thus high mass for low luminosities. Their extremely low metallicity argues for a very early epoch of star formation; this is confirmed by the colour-magnitude diagrams for some of the dwarf galaxies, which assign them an age of ~ 13 Gyr.

Warm dark matter as an alternative. The apparent conflict between the abundance of sub-halos and the observed satellite galaxies in the Milky Way can be potentially avoided if the initial power spectrum of density fluctuations has less power on small spatial scales – corresponding to masses of satellite galaxies. In particular, if a WDM particle has a mass of ~ 2 keV, the cut-off in the power spectrum would correspond to the halo mass of dwarf galaxies and all small-scale sub-halos effectively disappear.
However, observations of the Lyman-α forest strongly constrain the allowed mass range of WDM particles, and lower limits on the mass of WDM particles obtained from these studies come exceedingly close to the mass needed to substantially reduce the abundance of sub-halos.
Lecture note: For low enough mass DM halos, their time to cool is much larger than for high mass halos. Hence, they may not have fully cooled by this epoch of the universe in which case star formation hasn't occured at meaningful scales. I.e. we may not see these halos despite their possible existence. Further, the reionization of the universe may have disrupted the star formation in low mass halos in which case they may *never* undergo star formation.

Evidence for the presence of CDM substructure in galaxies. Gravitational lensing studies have provided strong constraints on the number and mass of sub-halos within lensing galaxies. This generally favours complex sub-halo structure, rather than a 'smooth', simple mass model consisting of few and sparse halos.

The 'disk of satellite galaxies'. Whereas the abundance of dark matter sub-halos in galaxies no longer presents a serious problem for CDM models of structure formation, the spatial distribution of satellite galaxies around the Milky Way requires more explanation. The 11 classical satellites

of the Milky Way seem to form a planar distribution. Such a distribution would be extremely unlikely if the satellite population was drawn from a near-isotropic probability distribution.
Using models of galaxy formation, the accretion of smaller mass halos onto a high-mass halo occurs predominantly in the direction of the filaments that galaxies preferentially form in within large scale structure. The most massive sub-halos therefore tend to form in a planar distribution, not unlike the one seen in the Milky Way's satellite distribution – solving the problem.

Ch 10.1 – Galaxy Evolution

Copied verbatim.
In the cold dark matter universe, small density structures formed first, which means that low-mass dark matter halos preceded those of higher mass. This 'bottom-up' scenario of structure formation follows from the shape of the power spectrum of density fluctuations, which itself is determined by the nature of dark matter—namely cold dark matter. The gas in these halos is compressed and heated, the source of heat being the potential energy. If the gas is able to cool by radiative processes, i.e., to get rid of some of its thermal energy and thus pressure, it can collapse into denser structures, and eventually form stars. In order for this to happen, the potential wells have to have a minimum depth, so the resulting kinetic energy of atoms is sufficient to excite the lowest-lying energy levels whose de-excitation then leads to the emission of a photon which yields the radiative cooling. We shall see that this latter aspect is particularly relevant for the first stars to form, since they have to be made of gas of primordial composition, i.e., only of hydrogen and helium.

Once the first stars form in the Universe, the baryons in their cosmic neighborhood get ionized. This reionization at first happens locally around the most massive dark matter halos that were formed; later on, the individual ionized regions begin to overlap, the remaining neutral regions become increasingly small, until the process of reionization is completed, and the Universe becomes largely transparent to radiation, i.e., photons can propagate over large distances in the Universe. The gas in dark matter halos is denser than that in intergalactic space; therefore, the recombination rate is higher there and the gas in these halos is more difficult to ionize. Probably, the ionizing intergalactic radiation has a small influence on the gas in halos hosting a massive galaxy. However, for lower-mass halos, the gas not only maintains a higher ionization fraction, but the heating due to ionization can be appreciable. As a result, the gas in these low-mass halos finds it more difficult to cool and to form stars. Thus, the star-formation efficiency—or the fraction of baryons that is turned into stars—is expected to be smaller in low-mass galaxies.

The mass of halos grows, either by merging processes of smaller-mass halos or by accreting surrounding matter through the filaments of the large-scale density field. The behavior of the baryonic matter in these halos depends on the interplay of various processes. If the gas in a halo can cool, it will sink towards the center. One expects that the gas, having a finite amount of angular momentum like the dark matter halo itself, will initially accumulate in a disk perpendicular to the angular momentum of the gas, as a consequence of gas friction—provided a sufficiently long time of quiescent evolution for this to happen. The gas in the disk then reaches densities at which efficient star formation can set in. In this way, the formation of disk galaxies, thus of spirals, can be understood qualitatively.

As soon as star formation sets in, it has a feedback on the gas: the most massive stars very quickly explode as supernovae, putting energy into the gas and thereby heating it. This feedback then prevents that all the gas turns into stars on a very short time-scale, providing a self-regulation mechanism of the star-formation rate. In the accretion of additional material from the surrounding of a dark matter halo, also additional gas is accreted as raw material for further star formation.

When two dark matter halos with their embedded galaxies merge, the outcome depends mainly on the mass ratio of the halos: if one of them is much lighter than the other, its mass is simply added to the more massive halo; the same is true for their stars. More specific, the small-mass galaxy is disrupted by tidal forces, in the same way as the Sagittarius dwarf galaxy is currently destroyed in our Milky Way, with the stars being added to the Galactic halo. If, on the other hand, the masses of the two objects are similar, the kinematically cold disks of the two galaxies are expected to be disrupted, the stars in both objects obtain a large random velocity component, and the resulting object will be kinematically hot, resembling an elliptical galaxy. In addition, the merging of gas-rich galaxies can yield strong compression of the gas, triggering a burst of star formation, such as we have seen in the Antennae galaxies. Merging should be particularly frequent in regions where the galaxy density is high, in galaxy groups for instance. A large number of such merging and collision processes are detected in galaxy clusters at high redshift.

In parallel, the supermassive black holes in the center of galaxies must evolve, as clearly shown by the tight scaling relations between black hole mass and the properties of the stellar component of galaxies. The same gas that triggers star formation, say in galaxy mergers, can be used to 'feed' the central black hole. If, for example, a certain fraction of infalling gas is accreted onto the black hole, with the rest being transformed into stars, the parallel evolution of black hole mass and stellar mass could be explained. In those phases where the black hole accretes, the galaxy turns into an active galaxy; energy from the active galactic nucleus, e.g., in the form of kinetic energy carried by the jets, can be transmitted to the gas of the galaxy, thereby heating it. This provides another kind of feedback regulating the cooling of gas and star formation.

When two halos merge, both hosting a galaxy with a central black hole, the fate of the black holes needs to be considered. At first they will be orbiting in the resulting merged galaxy. In this process, they will scatter off stars, transmitting a small fraction of their kinetic energy to these stars. As a result, the velocity of the stars on average increases and many of them will be 'kicked out' of the galaxy. Through these scattering events, the black holes lose orbital energy and sink towards the center of the potential. Finally, they form a tight binary black hole system which loses energy through the emission of gravitational waves until they merge.

The more massive halos corresponding to groups and clusters only form in the more recent cosmic epoch. In those regions of space where at a later cosmic epoch a cluster will form, the galaxy-mass halos form first—the larger-scale overdensity corresponding to the proto-cluster promotes the formation of galaxy-mass halos, compared to the average density region in the Universe; this is the physical origin of galaxy bias. Therefore, one expects the oldest massive galaxies to be located in clusters nowadays, explaining why most massive cluster galaxies are red. In addition, the large-scale environment provided by the cluster affects the evolution of galaxies, e.g., through tidal stripping of material.

Ch 10.2 – Gas in Dark Matter Halos

10.2.1 – The Infall of Gas During Halo Collapse

Gas Heating. As long as the fractional overdensities are small, the spatial distribution of baryons and dark matter are expected to be very similar in the very early halo formation. However, when the spherical halo collapses, the behaviour of both components must be very different: dark matter is collisionless and baryons are collisional (meaning that friction prevents gas from crossing through a gas distribution). Thus, as the halo collapses, the potential energy of the gas is transformed into heat through the frictional processes. Furthermore, the pressure of the gas can prevent it from falling into the dark matter potential well.
In the case of (approximate) spherical symmetry, the gas had already settled down in the inner part of the halo and gas pressure balances gravitational force. As the outer part of the halo collapses, gas falls onto this gas distribution. The infall speed is much higher than the sound velocity of the (cold) infalling gas, and a shock front develops. Inside this front, the gas is hot and almost all of its kinetic energy gets converted into heat.

Hence, a collapsed halo should contain hot gas with a temperature depending on the halo radius and mass. Such hot gas is seen in galaxy groups and clusters through X-ray emission. Galaxy mass halos have a characteristic gas temperature of $\sim 10^6$K and so are much more difficult to observe (since they're too cool to emit X-rays and most atoms are fully ionized at that temperature). Nevertheless, some significant fraction of the hot gas in galaxy-mass halos does not stay hot and must cool to form stars.

10.2.2 – Cooling of Gas

Optically thin gas can cool by emitting radiation, e.g. by scattering between electrons and nuclei in an ionized gas (bremsstrahlung) or collisional excitations (and relaxation and emission of photons).

Cooling function. Although elements heavier than helium have a small abundance in number, they can dominate the gas cooling due to the rich energy spectrum of many-electron atoms. Hence, more enriched gas finds it easier to cool.
Atomic gas cannot cool efficiently for temperatures $T \lesssim 10^4$K due to the lack of charged particles in the gas. Molecules, on the other hand, have a rich spectrum of energy levels at low temperatures and can lead to efficient cooling. This is why star formation occurs in molecular clouds, where gas can efficiently cool and thereby compress to high densities.

Cooling time. Once we know the rate at which gas loses its energy, we can calculate the cooling time (the time it takes the gas [at constant cooling rate] to lose all of its energy). If this cooling time is longer than the age of the Universe, then the gas essentially stays at the same temperature and is unable to collapse towards a halo center. For most regions within galaxy clusters, this is the case, and cooling is only efficient towards cluster centers.

Conditions for efficient cooling. If the cooling time is shorter than the free-fall time (given by equation (10.5)), then gas falls freely towards the center of a halo essentially unaffected by gas pressure.

$$t_{\rm ff} = \sqrt{\frac{3\pi}{32G\rho}} = \frac{\pi}{2}\sqrt{\frac{R^3}{2GM}} \tag{10.5}$$

If the cooling time is much longer than the free-fall time, the gas at *best* sinks to the center at a rate given by the cooling rate.

Difference between galaxies and groups/clusters. In sufficiently massive halos with $M_g \gtrsim 10^{12} M_\odot$, the small efficiency of gas cooling prevents gas from collapsing to the center and forming stars there. At smaller masses, cooling is effective to enable rapid gas collapse. This dividing line in mass is about the mass which distinguishes galaxies from groups and clusters. In the latter, only a small fraction of the baryons is turned into stars (and this is generally contained within the galaxies of the group). In contrast, a large fraction of baryons in galaxies is concentrated towards the center, as visible in their stellar distribution. Thus, the difference between galaxies and groups/clusters is their efficiency to turn baryons into stars, and this difference is explained with the different cooling efficiencies of matter halos (as in figure 10.4).

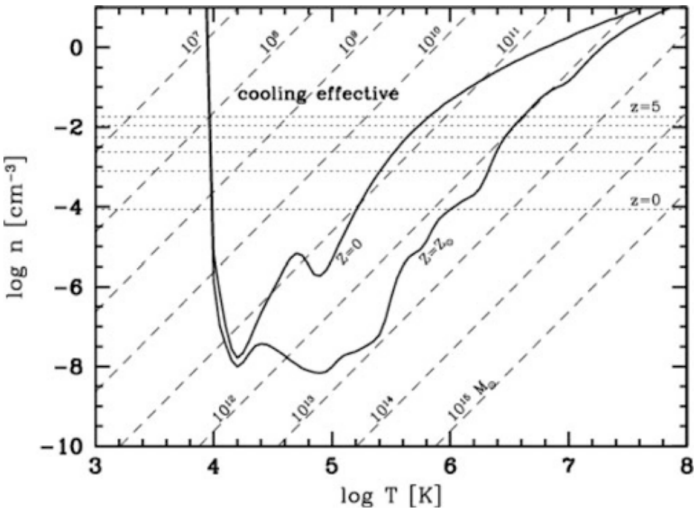

Figure 10.4: Solid curves are for gas metallicities of $Z = 0$ and $Z = Z_\odot$. Dotted lines show the density of halos formed at the specified redshifts. For gas densities and temperatures above the curve, cooling is efficient, whereas cooling time is longer than the free-fall time below the curves.

Low-mass halos. A halo with gas mass $\sim 10^{7.5} M_\odot$ lies inside the cooling curve only at *very* high redshift, i.e. when the corresponding density in a halo is very high. Therefore, gas can cool, and stars form, in halos of this mass only if they formed early enough. We therefore expect that the stars in such low-mass halos are very old.

Lecture notes

Plane of Satellites Problem. Most satellite galaxies discovered so far seem to be distributed in a plane more or less perpendicular to the disk of the Milky Way, despite ΛCDM simulations predicting they should be isotropically distributed. The angular momentum of the observed galaxies are closely aligned in the plane, and are mostly lining up with the large scale distribution of galaxies, hence filamentary accretion could be a possible explanation for their positions.

Cusp-Core Problem. Dwarf galaxy rotation curves seem to be better fitted by dark matter density profiles with central cores instead of cusps. Stellar feedback might provide a solution to this, though. As gas settles into the center of a galaxy and forms stars, much of the gas would then be expelled by supernova explosions, hence flattening the slope of the central dark matter profile as the baryonic matter interacts with the dark matter.

Week 6

Ch 10.3 – Reionization of the Universe

10.3.1 – The First Stars

Understanding reionization (currently understood to have occurred around $z \sim 10$) is directly linked to studying the first generation of stars.

The Jeans Mass. There exists a certain mass of a halo for which pressure forces are unable to prevent the infall of gas into a potential well,

$$M > M_J \equiv \frac{\pi^{5/2}}{6} \left(\frac{c_s^2}{G}\right)^{3/2} \frac{1}{\sqrt{\overline{\rho}}} \tag{10.6}$$

where $\overline{\rho}$ is the mean cosmic matter density, and c_s is the speed of sound in the gas. The Jeans mass depends on the temperature of the gas, expressed through the sound speed c_s. As a function of redshift, the Jeans mass can be calculated as

$$M_J = 5.7 \times 10^3 \left(\frac{\Omega_m h^2}{0.15}\right)^{-1/2} \left(\frac{\Omega_b h^2}{0.022}\right)^{-3/5} \left(\frac{1+z}{10}\right)^{3/2} M_\odot \tag{10.8}$$

Cooling of the Gas. The Jeans criterion is a necessary condition for the formation of proto-galaxies, i.e. dark matter halos which contain baryons. In order to form stars, the gas in the halos needs to be able to cool further. Here, we are dealing with the particular situation of the first galaxies, whose gas is metal-free, so metal lines cannot contribute to the cooling. The cooling function of primordial gas is much smaller than that of enriched material; in particular, the absence of metals means that even slow cooling through excitation of fine-structure lines cannot occur, as there are no atoms with such transitions present. Thus, cooling by the primordial gas is efficient only above $T \gtrsim 2 \times 10^4$K. Therefore, atomic hydrogen is a very inefficient coolant for these first halos, insufficient to initiate the formation of stars.

The importance of molecular hydrogen. Besides atomic hydrogen and helium, the primordial gas contained a small fraction of molecular hydrogen. Whereas in enriched gas, molecular hydrogen is formed on dust particles, and the primordial gas had no dust, and so H_2 must have formed in the gas phase itself (rendering its abundance very small). Despite its very small density, H_2 dominated the cooling rate of primordial gas at temperatures below $T \sim 10^4$K.
By means of H_2, the gas can cool in halos with a mass of $M \gtrsim 5 \times 10^4 M_\odot$ at $z \sim 20$. In these halos, stars may then be able to form. Such stars, which at the same mass presumably have a much higher temperature and luminosity (due to their zero metallicity) and thus a shorter lifetime, are called ***population III stars***. Due to their high temperature, they are much more efficient sources of ionizing photons than stars with 'normal' metallicity.

10.4.5 – The Formation and Evolution of Supermassive Black Holes

Black holes grow in mass by accreting material, a process we witness through the radiation from accreting black holes in AGN. There is no firm conclusion on how SMBHs initially formed, but three plausible formation scenarios have been studied in detail. We do know, however, that the first SMBHs must have formed early in the universe, as indicated by the presence of very luminous QSOs at $z > 6$.

Remnants of Population III Stars. The first stars formed out of primordial gas, i.e. gas with zero metallicity. The cooling properties of this gas are different from that of enriched material, since no metal lines are available for radiating energy away. It is expected that many stars can form with very high masses, well above $100M_\odot$; if the mass of a star is above $\sim 250M_\odot$, it will leave behind a black hole of mass $\gtrsim 100M_\odot$. Since these stars burn their nuclear fuel very quickly (exploding within a few million years), and are expected to first form at $z \gtrsim 20$, this formation mechanism would yield a very early population of seed black holes.

Gas-Dynamical Processes. Another route for the formation of SMBHs arises if the primordial gas in a high-redshift dark matter halo manages to concentrate in its center, through global dynamical instabilities (e.g. related to the formation of bar-like structures) that are able to transport angular momentum outwards. This angular momentum transport is needed since, otherwise, the central concentration of gas would be prevented by the angular momentum barrier. Subsequent cooling by molecular hydrogen may then lead to the formation of a rapidly rotating supermassive star with up to $10^6M_\odot$, provided the accumulation of gas occurs rapidly enough. Once the inner core of the supermassive star has burned its hydrogen, a black hole with mass of a few tens of $M_\odot$ would form (depending on the initial angular velocity of the star), which then subsequently accretes material from the outer layers of the star. Since quasi-spherical accretion has a low radiative efficiency, the BH can grow in mass quickly until it exceeds the Eddington luminosity and the remaining gas is expelled, leaving behind a SMBH with $\sim 10^5M_\odot$.

Stellar-Dynamical Processes. In the inner part of a forming galaxy, dense nuclear star clusters may form. Because of the high density, star-star collisions can occur which can lead to the formation of very massive stars in excess of $10^3M_\odot$. This has to happen very quickly (before the first stars explode in SNe) since otherwise the massive star would be polluted with metals, its opacity increased, and it would no longer be stable under its mass. The fate of this supermassive star is then similar to the scenario above, resulting in a black hole remnant of several hundred solar masses.

The above three scenarios are not mutually exclusive, and the current understanding of these processes is not sufficient to establish their likelihood and frequency.

Mass growth. Once the seek black holes have formed, they can grow in mass by accreting material. The characteristic time-scale for mass growth is the time by which the mass can double i.e.

$$\epsilon t_{\rm gr} = \frac{\epsilon M_\bullet c^2}{L_{\rm edd}} \approx 5\epsilon \times 10^8 \text{ yr}$$

With $\epsilon \sim 0.1$, a $10^4M_\odot$ seed black hole formed at $z \sim 20$ could grow to a few $\times 10^8M_\odot$ by $z \sim 7$ if accreted continuously at the Eddington rate. The situation is more difficult for seed black holes formed from population III stars; they probably require super-Eddington rates to be able to power the luminous QSOs at $z > 6$, which is possible but likely not for long time-scales or by large factors.

Ch 4.1 – Cosmology Introduction and Fundamental Observations

Cosmological observations are difficult in general, simply because the majority of the universe is very far away from us. Distant light sources are very dim, and so our knowledge of the universe runs parallel with the development of more advanced telescopes.

The finite speed of light in a Euclidean space, in which we are located at the origin $r = 0$ today ($t = t_0$), implies that we can only observe points in spacetime for which $|r| = c(t_0 - t)$. This implies that we can't observe any point in spacetime, and the set of points which satisfy that relation are called our *backward light cone*.

4.1.1 - Fundamental Cosmological Observations

a. The sky is dark at night (Olbers' paradox)

b. Averaged over large angular scales, faint galaxies are uniformly distributed across the sky.

c. With the exception of a very few nearby galaxies, a redshift is observed in the spectra of galaxies — most galaxies are moving away from us, with their velocity increasing linearly with distance.

d. In nearly all baryonic cosmic objects, the mass fraction of helium is 25-30%.

e. The oldest star clusters in our Galaxy have an age of ~ 12 Gyr.

f. A microwave radiation (CMBR) is observed, reaching us from all directions. This radiation is isotropic except for very small fluctuations with amplitude $\sim 10^{-5}$.

g. The spectrum of the CMBR corresponds, within very small error bars, to that of a perfect blackbody of a temperature $T_0 = 2.728 \pm 0.004$ K.

h. The number counts of radi sources at high Galactic latitude does *not* follow the simple law $N(> S) \propto S^{-3/2}$

4.1.2 - Simple Conclusions

Start with the assumption of an infinite, on-average homogeneous, Euclidean, static universe.

Olbers' paradox (1): In this assumed universe, the sky would be uncomfortably bright. With these assumptions, there would be a uniform spatial density of stars throughout the whole universe; in a spherical shell twice as far away, there would be four times as many stars (and so on). This implies that the universe would be filled with equally dense volumes of stars, and so the sky would be filled with starlight of temperature on the order of 10^4 K or above. This is obviously not the case.

Source Counts (8): Consider a population of light sources with a luminosity function that is constant in space and time. In a spherical shell, we would expect the counts of sources with flux $F > S$ to follow $N(> S) \propto S^{-3/2}$. This is in contradiction to observations.

From these two contradictions — Olbers' paradox and the non-Euclidean source counts — we conclude that at least one of the underlying assumptions of this universe must be wrong; our Universe cannot be all four of Euclidean, homogeneous, infinite, and static. The Hubble flow, i.e., the redshift of galaxies, indicates that the assumption of a static Universe is wrong.

The Age of Globular Clusters (5): requires that the Universe is at least 12 Gyr old, as it cannot be younger than the objects it contains. The age estimates for globular clusters yield values which are very close to the ***Hubble time*** $H_0^{-1} = 9.78h^{-1}$ Gyr. This suggests that the Hubble expansion may be directly linked to the evolution of the universe.

The apparently isotropic **distribution of galaxies (2)** when averaged over large scales, and the **CMBR isotropy (6)** suggest that the Universe is isotropic over large angular scales. If we assume, in addition, that our place in the cosmos is not privileged over any other place, then the assumption of isotropy around us implies that the Universe appears isotropic as seen from any other place. The homogeneity of the Universe follows immediately from the isotropy about every location.
The combined assumption of homogeneity and isotropy of the Universe is also known as the ***cosmological principle***.

The assumption of homogeneity breaks down at small scales, of course, due to galaxies, galactic clusters, galactic superclusters, etc. Large scale structures have been found that extend over $\sim 100h^{-1}$ Mpc (where $h = H_0$ in units of 100km/s/Mpc), but no indication of structures much larger than this. This length-scale can be compared to a characteristic length of the universe. This ***Hubble radius***, the characteristic length-scale of the observable Universe, is found by

$$R_H \coloneqq \frac{c}{H_0} = 2998h^{-1} \text{ Mpc} \tag{4.3}$$

The Hubble volume found from a sphere of Hubble radius can contain a very large number of structures of size $\sim 100H^{-1}$ Mpc, so it still makes sense to assume an on-average homogeneous cosmological model.

Ch 4.2 – An Expanding Universe

Only gravitational forces and electromagnetic forces can act over large distance. Since cosmic matter is electrically neutral on average, electromagnetic forces do not play any significant role on large scales; gravity has to be considered as the driving force in cosmology.

4.2.2 - Kinematics of the Universe

Comoving Coordinates: Consider a homogeneous sphere which may be radially expanding (or contracting), requiring that the density $\rho(t)$ be spatially homogeneous. The density may vary in time due to expansion or contraction. For some coordinate, $\boldsymbol{x}$, in this radially expanding sphere with radius from the origin of r at $t = t_0$, the radius at time t of this coordinate is

$$r(t) = a(t)\boldsymbol{x} \tag{4.4}$$

Since $\boldsymbol{x}$ and r both have the dimension of a length, $a(t)$ is dimensionless and only depends on time and is spatially constant. The function $a(t)$ is called the ***cosmic scale factor***, with $a(t_0) = 1$. Particles which move according to (4.4) are called comoving particles.

Expansion Rate: The velocity of a comoving particle is obtained by

$$\boldsymbol{v}(r,t) = \dot{a}\boldsymbol{x} = \frac{\dot{a}}{a}r \equiv H(t)r \tag{4.6}$$

where the ***expansion rate*** is

$$\boxed{H(t) \coloneqq \frac{\dot{a}}{a}} \tag{4.7}$$

Equation 4.6 yields a result strikingly similar to the Hubble law

$$\boxed{v = H_0 D} \tag{4.9}$$

where D is the distance to an object. These three equations express the fact that any observer expanding with the sphere will observe an isotropic velocity field that follows the Hubble law. Since we are observing an expansion today, we have $H_0 > 0$ and $\dot{a}(t_0) > 0$.

Ch 4.4 – Thermal History of the Universe

4.4.8 – Summary

Copied verbatim.

- Our Universe originated from a very dense, very hot state in the ***Big Bang***. Shortly afterwards, it consisted of a mix of various elementary particles, all interacting with each other.

- We are able to examine the history of the universe in detail, starting at an early epoch where it cooled down by expansion such as to leave only those particle species known to us, and probably a dark matter particle.
- Because of their weak interaction and the decreasing density, the neutrinos experience only little interaction at temperatures below $\sim 10^{10}$K, their decoupling temperature.
- at $T \sim 10^9$K, electrons and positrons annihilate into photons. At this low temperature, pair production ceases to take place.
- Protons and neutrons interact and form deuterium nuclei. As soon as $T \sim 10^9$K, deuterium is no longer efficiently destroyed by energetic photons. Further, nuclear reactions produce mainly helium nuclei. About 25% of the mass in nucleons is transformed into helium, and traces of lithium are produced, but no heavier elements.
- At about $T \sim 3000$K, some 400,000 years after the Big Bang, the protons and helium nuclei combine with the electrons, and the universe becomes essentially neutral (we say that is ***recombines***). From then on, photons can travel without further interactions. At recombination, the photons follow a blackbody distribution. By the ongoing cosmic expansion, the temperature of the spectral distribution decreases, $T \propto (1+z)$, though its Planck property remains.
- After recombination, the matter is the Universe is almost completely neutral. However, we know from the observation of sources at very high redshift that the intergalactic medium is essentially fully ionized at $z \lesssim 6$. Before $z > 6$, our Universe must there have experienced a phase of reionization. This effect cannot be explained in the context of the *strictly homogeneous* world models; rather it must be examined in the context of structure formation in the Universe and the formation of the first stars and AGN.

Ch 4.5 – Achievements and Problems of the Standard Model

4.5.2 – Problems

Despite the achievements of the standard model, there are some aspects which require further consideration.

The Horizon Problem: Since no signal can travel faster than light, the CMB radiation from two directions separated by more than about one degree originates in regions that were not in causal contact before recombination, i.e. the time when the CMB photons interacted with matter the last time. Therefore, these two regions have never been able to exchange information, for example about their temperature. Nevertheless, their temperature is the same, as seen from the high degree of isotropy of the CMB (which shows relative fluctuations of only $\Delta T/T \sim 10^{-5}$).

The Flatness Problem: For the total density parameter to be of order unity today, it must have been extremely close to 1 at earlier times, which means that a very precise 'fine tuning' of this parameter was necessary.

The above also suggests that the curvature term has never had a dominant effect on the universe.

4.5.3 – Extension of the Standard Model: Inflation

For all of the cosmological parameters to be the value that they are today (and with them, the universe not collapsing/rapidly expanding so that we see it in its current state today) is unlikely from a random standpoint. Different parameters could have led to the universe recollapsing billions of years ago or expanding so rapidly that no structure could be formed. These parameters come down to the initial conditions of the universe just after the Big Bang. The only answer to why these parameters are the values that they are today lies in some processes that must have taken place even earlier in the universe, and so the initial conditions of the normal Friedmann-Lemaitre expansion have a physical origin. Cosmologists believe they have found such a physical reason in the inflationary model.

Inflation. Physical laws and properties of elementary particles are well known up to energies of $\sim$ 100 GeV because they have been experimentally tested in particle accelerators. For higher energies, particles and their interactions are unknown. This means that the history of the Universe can only be considered secure up to this 100 GeV energy. The extrapolation to earlier times, up to the Big Bang, is considerably less certain. From particle physics, we expect new phenomena to occur at an energy scale of the Grand Unified Theories (GUTs), at about 10^{14} GeV, corresponding to $t \sim 10^{-34}$s.
In the inflationary scenario, it is presumed that at very early times the vacuum energy density was much higher than today, and so it dominated the Hubble expansion. Because of this, there would have been exponential expansion (inflationary phase), but only for a brief period. We assume that a phase transition took place in which the vacuum energy density is transformed into normal matter and radiation (a process called reheating), which ends the inflationary phase and after which the normal Friedmann evolution of the Universe begins.

Inflation solves the Horizon Problem. During inflation, the Hubble parameter is constant and so the horizon may become arbitrarily large in the inflationary phase (dependent on the duration of the exponential expansion). According to this scenario, the whole universe visible today was in causal contact prior to inflation, so that the homogeneity of the physical conditions at recombination, and with it the nearly perfect isotropy of the CMB, is provided by causal processes.

Inflation solves the Flatness Problem. Due to the tremendous expansion, any initial curvature is straightened out. Formally, during the inflationary phase we

have

$$\Omega_\Lambda = \frac{\Lambda}{3H^2} = 1$$

and since it is assumed that the inflationary phase lasts long enough for the vacuum energy to be completely dominant, when it ends we then have $\Omega_0 = 1$. Hence the universe is flat to an extremely good approximation.

Week 7

Ch 7.2 – Gravitational Instability

7.2.1 – Overview

The smallness of the CMB anisotropy suggests that the density inhomogeneities at redshift $z \sim 1000$ (the epoch where most CMB photons interacted with matter for the last time) must have had very small amplitudes. Today, the amplitudes of the density inhomogeneities are considerably larger (due to structure growth and contraction), and there are generally no longer small density fluctuations.
The universe becomes more inhomogeneous in the course of its evolution, since density perturbations grow over time. We can define the ***relative density contrast*** as

$$\delta(\mathbf{r}, t) \equiv \frac{\rho(\mathbf{r}, t) - \overline{\rho}(t)}{\overline{\rho}(t)} \tag{7.1}$$

where $\overline{\rho}(t)$ denotes the mean cosmic matter density at time t. The smallness of the CMB anisotropy suggests that $|\delta| \ll 1$ at $z \sim 1000$. The dynamics of the cosmic Hubble expansion is controlled by the gravitational field of the average matter density $\overline{\rho}(t)$, whereas the density fluctuations generate an additional gravitational field.

Density fluctuations grow over time due to their self-gravity; overdense regions increase their density contrast over the course of time, while underdense regions decrease their density contrast. In both cases, $|\delta|$ increases. Hence, this effect of ***gravitational instability*** leads to an increase of density fluctuations with increasing time. The evolution of structure in the universe is described by this effect of gravitational instability.

7.2.2 – Linear Perturbation Theory

The Hubble Expansion. The Hubble expansion of

$$\mathbf{v}(\mathbf{r}, t) = H(t)\mathbf{r}$$

satisfies the Poisson equation for the gravitational potential if ρ is homogeneous and the Friedmann equation for the scale factor applies. As long as the density contrast $|\delta| \ll 1$, the deviations of the velocity field from the Hubble expansion will be small.
It is convenient to consider the problem in comoving coordinates, hence define

$$\mathbf{r} = a(t)\mathbf{x}$$

In a homogeneous cosmos, $\mathbf{x}$ is a constant for every matter particle, and its spatial position $\mathbf{r}$ changes only due to the Hubble expansion. Likewise, the velocity field is then written in the form

$$\mathbf{v}(\mathbf{r}, t) = \frac{\dot{a}}{a}\mathbf{r} + \mathbf{u}\left(\frac{\mathbf{r}}{a}, t\right) \tag{7.5}$$

where $\mathbf{u}(\mathbf{x}, t)$ is a function of the comoving coordinate $\mathbf{x}$. The first term represents the homogeneous Hubble expansion, whereas the second term describes the deviations from this homogeneous expansion. For this reason, $\mathbf{u}$ is called the *peculiar velocity*.

The Growth Factor. The density contrast at some comoving coordinate $\mathbf{x}$ as a function of time can be represented in terms of a growth factor,

$$\delta(\mathbf{x}, t) = D_+(t)\delta_0(\mathbf{x}) \tag{7.16}$$

This tells us that the spatial shape of density fluctuations are frozen in comoving coordinates, and only their amplitude increases with time.
For any cosmological model, the growth factor can be found by

$$D_+(a) \propto \frac{H(a)}{H_0} \int_0^a \frac{da'}{\left[\Omega_m a'^{-1} + \Omega_\Lambda a'^2 - (\Omega_m + \Omega_\Lambda - 1)\right]^{3/2}} \tag{7.17}$$

where the factor of proportionality is determined from the condition $D_+(t_0) = 1$. In accordance with this, $\delta_0(\mathbf{x})$ would be the distribution of density fluctuations today if the evolution was linear until the present epoch. Therefore, $\delta_0(\mathbf{x})$ is denoted as the *linearly extrapolated density fluctuation field*.

Evidence for Dark Matter on Cosmic Scales. At the present epoch, $\delta \gg 1$ on scales of clusters of galaxies ($\sim$ 2Mpc), and $\delta \sim 1$ on scales of superclusters ($\sim$ 10Mpc). Hence, the law of linear structure growth (eq. 7.16) and the behaviour of $D_+(t)$ would mean that $\delta \gtrsim 10^{-3}$ at $z = 1000$ for these structures to be able to grow to non-linear structures at the present epoch. For this reason, we should also expect CMB fluctuations to be of comparable magnitude, $\Delta T/T \gtrsim 10^{-3}$. The observed fluctuation amplitude is much smaller, $\Delta T/T \sim 10^{-5}$, however, and so the corresponding density fluctuations cannot have grown sufficiently strongly up to today to form non-linear structures.
This contradiction can be resolved by the dominance of dark matter. Since photons interact with baryonic matter only, the CMB anisotropies basically provide information on the density contrast of *baryons*. Dark matter may have had a higher density contrast at recombination, but the baryons, which are strongly coupled to the radiation field before recombination, are prevented from strong clustering due to the radiation pressure. Only after recombination, when the electrons have combined with the atomic nuclei and essentially no free electrons remain, the coupling to the radiation field ends, after which the baryons may fall into the potential wells formed by the dark matter.

Lecture note: Inflation Yielding Temperature Fluctuations. Inflation prevents the CMB from having large temperature fluctuations of $\delta T/T \sim 1$. On the other hand, by inflating quantum perturbations to macroscopic

scales, inflation also causes the observed small temperature fluctuations of $\delta T/T \sim 10^{-5}$. How can quantum fluctuations (QF) give rise to temperature fluctuations? One patch of spacetime might end inflation early, will reheat, enter the radiation era and start cooling down, while another patch is still in its inflationary period and is not cooling down yet. Thus, when the inflation re-heating phase is over, those QF will resolve in small differences in temperature.

Ch 7.3 – Description of Density Fluctuations

We can at best hope to predict the statistical properties of the mass distribution in the universe, rather than having an analytical solution at every spatial point. How can the statistical properties of a density field best be described?
Two universe are considered equivalent if their density fields δ have the same statistical properties. One may then imagine considering a large (statistical) ensemble of universes whose density fields all have the same statistical properties, but for which the individual functions $\delta(\mathbf{x})$ can all be different. This statistical ensemble is called a *random field*, and any individual distribution with the respective statistical properties is called a realization of the random field.

7.3.1 – Correlation Functions

Galaxies are not randomly distributed in space, but rather they gather in groups, clusters, or large scale structure. This means that the probability of finding a galaxy at location $\mathbf{x}$ is not independent of whether there is a galaxy at a neighbouring point $\mathbf{y}$. It is more probable to find a galaxy in the vicinity of another that at an arbitrary location. Consider two points $\mathbf{x}$ and $\mathbf{y}$, and the two volume elements dV around these points. If $\overline{n}$ is the average number density of galaxies, the probability of finding a galaxy in the volume element dV around $\mathbf{x}$ is then

$$P_1 = \overline{n}\, dV$$

independent of $\mathbf{x}$ if we assume that the universe is statistically homogeneous. We choose dV such that $P_1 \ll 1$, so that the probability of finding two or more galaxies in the volume is negligible.
The probability of finding a galaxy in the volume element dV at location $\mathbf{x}$ and at the same time finding a galaxy in the volume element dV at location $\mathbf{y}$ is then

$$P_2 = (\overline{n}\, dV)^2[1 + \xi_g(\mathbf{x}, \mathbf{y})] \tag{7.26}$$

If the distribution of galaxies was uncorrelated, the probability P_2 would simply be the product of the probabilities of finding a galaxy at each of the locations $\mathbf{x}$ and $\mathbf{y}$ in a volume element dV (i.e. $P_2 = P_1^2$). But since the distribution is correlated, the relation needs to be modified to include the ***two-point correlation function*** of galaxies $\xi_g(\mathbf{x}, \mathbf{y})$.
By analogy to this, the correlation function for the total matter density can be defined as

$$\langle \rho(\mathbf{x})\rho(\mathbf{y})\rangle \equiv \overline{\rho}^2\ [1 + \xi(\mathbf{x}, \mathbf{y})] \tag{7.27}$$

where the angular brackets denote averaging over an ensemble of distributions that have the same statistical properties. Since the universe is considered statistically homogeneous, ξ can only depend on the difference $\mathbf{x} - \mathbf{y}$ and not on $\mathbf{x}$ and $\mathbf{y}$ individually. Further, ξ can only depend on the separation $r = |\mathbf{x} - \mathbf{y}|$ and not on the direction of the separation vector because of the assumed statistical isotropy of the universe. Thus, $\xi = \xi(r)$ is simply a function of the separation between two points.

By spatial averaging, the galaxy correlation function was found as

$$\xi_g(r) = \left(\frac{r}{r_0}\right)^{-\gamma} \tag{7.28}$$

for galaxies of luminosity $\sim L^*$, where $r_0 \simeq 5h^{-1}$Mpc is the correlation length, and the slope is $\gamma \simeq 1.7$. This relation is valid over a range $0.2h^{-1}\text{Mpc} \lesssim r \lesssim 30h^{-1}\text{Mpc}$.

The correlation function provides a means to characterise the structure of the cosmological matter distribution.

7.3.2 – The Power Spectrum

An alternative (and equivalent) description of the statistical properties of a random field, and thus of the matter distribution in a universe, is the power spectrum $P(k)$. Roughly speaking, the power spectrum describes the level of structure as a function of the length-scale $L \simeq 2\pi/k$; the larger $P(k)$ is, the larger the amplitude of the fluctuations on a length scale of $2\pi/k$. Here, k is a comoving wave number.
Phrased differently, the density fluctuations are decomposed into a sum of plane waves of the form

$$\delta(\mathbf{x}) = \sum a_{\mathbf{k}}\, \cos(\mathbf{x} \cdot \mathbf{k})$$

with a wave vector $\mathbf{k}$ and an amplitude $a_{\mathbf{k}}$. The power spectrum $P(k)$ then describes the mean of the squares of the amplitudes, $|a_{\mathbf{k}}|^2$, averaged over all wave vectors with equal length $k = |\mathbf{k}|$.
The power spectrum and correlation function are related through a Fourier transform, and both are used interchangeably in cosmology.

Gaussian Random Fields. In general, knowing the power spectrum is not sufficient to unambiguously describe the statistical properties of any random field. However, for certain classes of random fields, this is different. In fact, Gaussian random fields are uniquely characterised by $P(k)$. Among the properties which characterise them, the probability distribution of the density fluctuations $\delta(\mathbf{x})$ at any point is a Gaussian. Such Gaussian random fields play an important role in cosmology because it is assumed that at very early epochs, the density field obeyed Gaussian statistics (an assumption backed by the anisotropies in the CMB).
Lecture note: Since the density fluctuations are created by inflation, we expect the density field to be a Gaussian random field.

Ch 7.4 – Evolution of Density Fluctuations

$P(k)$ and $\xi(r)$ both depend on cosmological time or redshift, because the density field in the universe evolves over time. Therefore, the dependence on t is explicitly written as $P(k,t)$ and $\xi(r,t)$. Note that $P(k,t)$ is linearly related to $\xi(r,t)$, and ξ in turn depends quadratically on the density contrast δ. If $\mathbf{x}$ is the comoving separation vector, we then know the time dependence of the density fluctuations, $\delta(\mathbf{x},t) = D_+(t)\delta_0(\mathbf{x})$. So,

$$\xi(r,t) = D_+^2(t)\xi(r,t_0) \tag{7.30}$$

$$P(k,t) = D_+^2(t)P(k,t_0) \equiv D_+^2(t)P_0(k) \tag{7.31}$$

These relations are only valid in the Newtonian, linear perturbation theory in the matter dominated era of the universe.

7.4.1 – The Initial Power Spectrum

The Harrison-Zeldovich Spectrum. At early times, the expansion of the universe follows a power law, $a(t) \propto t^{1/2}$ in the radiation dominated era. At that time, no natural length-scale existed in the universe to which one might compare a wavelength. The only mathematical function that depends on a length but does not contain any characteristic scale is a power law; hence for very early times one should expect

$$P(k) \propto k^{n_s} \tag{7.32}$$

Harrison, Zeldovich, Peebles and others argued that $n_s = 1$, where the amplitude of the fluctuations of the gravitational potential are constant, i.e. preferring neither small nor large scales. For this reason, the spectrum with $n_s = 1$ is called a scale-invariant spectrum. With such a spectrum, we may choose a time t_i after the inflationary epoch and write

$$P(k,t_i) = D_+^2(t_i)Ak^{n_s} \tag{7.33}$$

where A is a normalisation constant fixed by observations. This, however, needs to be modified to account for the different growth of the amplitude of density fluctuations in the radiation-dominated epoch (compared to the later cosmic epochs from which it was derived).

Cold and Hot Dark Matter. The aforementioned modifications depend on the nature of dark matter. We differentiate ***cold dark matter*** (CDM) and ***hot dark matter*** (HDM) based on their characteristic velocities. CDM has a velocity dispersion that is negligible compared to astrophysically relevant velocities. Therefore, their initial velocity dispersion can well be approximated by zero, and all dark matter particles have the bulk velocity $\mathbf{u}$ of the cosmic 'fluid'. In contrast, the velocity dispersion of hot dark matter is appreciable. Neutrinos are the best candidate for HDM, and their characteristic velocity is specified by their rest mass, which prevents them from forming matter concentrations at all mass scales except for the most massive ones, as their velocity is larger than the corresponding escape velocities.

7.4.2 – Growth of Density Perturbations and the Transfer Function

The Transfer Function. The power spectrum $P(k)$ is affected by the nature of dark matter, and so we modify the power spectrum by including a transfer function $T(k)$, in the form

$$P(k,t) = D_+^2(t)Ak^{n_s}T^2(k) \tag{7.35}$$

where $T(k)$ depends on the nature of dark matter.

CDM and HDM. In HDM models, small-scale fluctuations are washed out by free-streaming of relativistic particles, i.e. the power spectrum is completely suppressed for large k, which is expressed by the transfer function $T(k)$ decreasing exponentially for large k. In the context of such a theory, large structures will form first, and galaxies can form only later by fragmentation of large structures. This scenario is in clear contradiction to observations, since we observe galaxies and QSOs at $z > 6$ so that small-scale structure is already present at times when the universe was only 10% of its current age. In addition, both in the local universe and at high redshift, the observed correlation function of galaxies is incompatible with cosmological models in which the dark matter is composed mainly of HDM.
Therefore, we can exclude HDM as the dominant constituent of dark matter, and we assume that the dark matter is 'cold'.

Qualitative Behaviour of the Transfer Function. The behaviour of the growth of a density perturbation on a scale L for $z < z_{\rm center}(L)$ depends on $z_{\rm center}$ itself. If a perturbation enters the horizon in the radiation-dominated phase, $z_{\rm eq} \lesssim z_{\rm center}(L)$, it ceases to grow during the epoch $z_{\rm eq} \lesssim z \lesssim z_{\rm center}(L)$. In this period, the energy density in the universe is dominated by radiation, and the resulting expansion rate prevents an efficient perturbation growth. At later epochs, when $z \lesssim z_{\rm eq}$, the growth of density perturbations continues. If $z_{\rm center}(L) \lesssim z_{\rm eq}$, that is if the perturbation enters the horizon during the matter-dominated epoch of the universe, these perturbations will grow as described earlier with $\delta \propto D_+(t)$. This implies that a length scale L_0 is singled out, namely the one for which

$$z_{\rm eq} = z_{\rm center}(L_0) \tag{7.37}$$

so that L_0 is the comoving horizon size at matter-radiation equality. This length scale is

$$L_0 \approx 16(\Omega_m h^2)^{-1}\ \text{Mpc} \tag{7.39}$$

Density fluctuations with $L > L_0$ enter the horizon after matter started to dominate the energy density of the universe; hence their growth is not impeded by a phase of radiation dominance. In contrast, density fluctuations with $L < L_0$ enter the horizon at a time when radiation was still dominating. These then cannot grow further as long as $z > z_{\rm eq}$, and only in the matter dominated epoch will their amplitudes proceed to grow again. Their relative amplitude up to the present time has therefore grown by a smaller factor than that of fluctuations with $L > L_0$.

In the limiting cases of $L \gg L_0$ and $L \ll L_0$, we get

$$T(k) \approx \begin{cases} 1 & k \ll 1/L_0 \\ (kL_0)^{-2} & k \gg 1/L_0 \end{cases} \tag{7.40}$$

7.4.3 – The Baryonic Density Fluctuations

The evolution of density fluctuations of baryons differs from that of dark matter. The reason for this is essentially the interaction of baryons with photons: although matter dominates the universe for $z < z_{\rm eq}$, the energy density of baryons remains smaller than that of the photons for a longer time; if radiation-matter equality happens at $z \sim 3000$, then the photon density is larger than that of baryons for $z \gtrsim 800$.
Since photons and baryons interact with each other by photon scattering on free electrons, which are tightly coupled electromagnetically to protons and helium nuclei, baryons and photons are strongly coupled before recombination, forming a single fluid. Due to the presence of photons, this fluid has a strong pressure which prevents it from falling into potential wells formed by the dark matter. Thus, this pressure prevents strong inhomogeneities of the baryon-photon fluid.

Sound Waves. Consider again a perturbation of comoving scale L: as long as this perturbation is larger than the horizon size, pressure effects can not affect the behaviour of the fluid and so baryons and photons behave in the same way as the dark matter – the amplitude of their perturbations grow. As soon as the perturbation enters the horizon, pressure provides a restoring force against the gravitational effect of the dark matter density maxima, essentially acting against a compression of the baryon-photon fluid. As a result, this fluid will develop sound waves.

Sound Horizon. The maximum distance sound waves can travel up to in a given epoch is called the sound horizon. Loosely speaking, it is given by the product of the sound speed and the cosmic time and acts essentially as an event horizon. The sound speed in this photon-dominated fluid is given by $c_s \approx c/\sqrt{3}$ and so the sound horizon is about a factor of $\sqrt{3}$ smaller than the event horizon. As soon as the perturbation enters the sound horizon, the amplitude of the baryon-photon fluctuations can not grow anymore and instead undergo damped oscillations.
At recombination, the free electrons recombine with the hydrogen and helium nuclei, after which there are essentially no more free electrons which couple to the photon field. Hence, after recombination the baryon fluid lacks the pressure support of the photons and the sound speed drops to zero – the sound waves no longer propagate and get frozen in. Now the baryons are free to react to the gravitational field created by the dark matter inhomogeneities, and they can fall into their potential wells. After some time, the spatial distribution of the baryons is essentially the same as that of the dark matter.

Baryonic Acoustic Oscillations. The sound waves in the baryon-photon fluid, the BAOs, are observable today. Since at recombination the photons interacted with matter for the last time, the cosmic microwave background radiation provides us with a picture of the density fluctuations at the epoch of recombination.

BAOs in the Low-Redshift Universe. The baryons, once no longer coupled to the radiation and become pressureless, fall into the potential wells of dark matter. This is because the dark matter fluctuations can grow while the baryonic fluctuations could not due to the photon pressure, and because the mean density of dark matter is substantially larger than that of the baryons. However, the density of baryons is $\sim 15\%$ of the total matter density and so isn't completely negligible. As a result, a small fraction of the matter also follows the inhomogeneities created by the frozen standing waves of the baryons. Since these waves have a characteristic length scale – the sound horizon at recombination – this characteristic length scale should be visible in the properties of the matter distribution even today.

Lecture notes: For perturbation growth, we obtain

$$\ddot{\delta} + 2H(t)\dot{\delta} = 4\pi G\overline{\rho}(t)\delta(t)$$

On the left, the Hubble expansion $H(t)$ suppresses perturbation growth by driving down the matter density with a timescale of $1/H(t)$. On the right, the self-gravity term increases the density with time. If the universe is dense, gravity will tend to make it denser. The time scale for this perturbation growth is $t_d \sim (G\rho)^{-1/2}$. I.e. if matter is not dominant, then perturbations grow extremely slowly. Conversely, if matter is dominant, perturbations grow as a power law (self gravity and expansion contrast each other, and so this is not exponential growth).
We are now entering the Λ dominated era, and so the biggest collapsing objects that we see today (superclusters) are the biggest inhomogeneities we'll ever see (for dark matter).

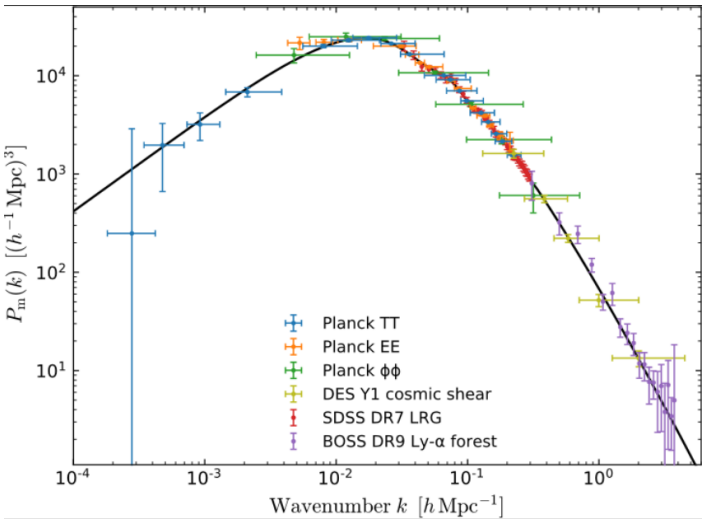

Different size perturbations 'enter' the horizon at different times. Outside the horizon, all fluctuations grow the same. Inside the horizon, the growth depends on the time the perturbations enter: before matter domination, there's no growth in the matter perturbations, after matter domination,

the growth is proportional to a. This creates a characteristic scale in the clustering of matter: $k_{\rm eq} \propto \Omega_m h^2$.

Week 8

Ch 8.6 – Angular Fluctuations of the CMB

The angular distribution of the CMB temperature reflects the matter inhomogeneities at the redshift of decoupling of radiation of matter.

8.6.1 – Origin of the Anisotropy: Overview

The CMB anisotropies reflect the conditions in the universe at the epoch of recombination at $z \sim 1100$. Temperature fluctuations originating at this time are called ***primary anisotropies***. Later, as the CMB photons propagate through the universe, they may experience a number of distortions along their way which may change their temperature distribution across the sky. These are called ***secondary anisotropies***.

Primary anisotropies. The most basic mechanisms causing primary anisotropies can be divided into those which occur on scales larger than the horizon size at recombination (i.e. which can not have been affected by physical interactions up to the time of last scattering) and those on smaller scales.

- Inhomogeneities in the gravitational potential cause photons which originate in regions of higher density to climb out of a potential well, and are consequently gravitationally redshifted. This is slightly compensated by the time-dilation induced by the well scattering photons from earlier times and correspondingly higher temperatures. These effects are combined under the term *Sachs-Wolfe effect*.
- Peculiar velocities of electrons from the last CMB scattering are subject to a doppler shift from our perspective, which can induce a direction-dependent temperature change.
- On scales larger than the horizon scale, the baryon density is enhanced by association with dark matter, and so there is an increased temperature of baryons in overdense regions.

Inside the sound horizon, two other effects dominate the primary anisotropy signal:

- The baryon-photon fluid are closely coupled before recombination, and so the density peaks of the sound waves feature an adiabatically compressed baryon-photon fluid which is hotter than the average. This gives a characteristic length or angular scale for temperature fluctuations.
- The coupling of baryons and photons is not perfect, since they are decoupled on very small spatial scales. As such, the temperature fluctuations can be smeared by diffusion of photons on scaled below about $\sim 5'$ (*Silk damping*), and so only very small fluctuations exist on this scale.

Secondary Anisotropies.

- Thomson scattering of CMB photons in the $1000 \lesssim z \lesssim 6$ universe by reionized, free electrons means that we observe a fraction $f_{\rm sc}$ of scattered photons and $(1-f_{\rm sc})$ unscattered electrons. The amplitude of the measured temperature anisotropies needs to be corrected for that scatter proportion.
- Photons propagating towards us are traversing a universe with structure formation, and hence a time-varying gravitational potential. As such, they are subjected to anisotropic blueshifting (except in an Einstein-de Sitter model) and this effect works somewhat against the initial gravitational redshift to give the *integrated Sachs-Wolfe effect (ISW)*.
- The gravitational deflection of CMB photons, caused by the gravitational field of the cosmic density fluctuations, leads to a change in photon direction (gravitational lensing), and so the correlation function can be slightly smeared out on small angular scales.
- The Sunyaev-Zeldovich effect describes the scattering of CMB photons off of hot gas in intracluster media, in which case the measured intensity of low-frequency CMB light is reduced, and increased at high frequencies. This changes the observed Planck spectrum, unlike the ISW and gravitational lensing effects.

8.6.2 – Description of the CMB Anisotropy

We can describe relative temperature fluctuations as $\mathcal{T}(\mathbf{n}) = [T(\mathbf{n}) - T_0]/T_0$, where $\mathbf{n}$ is a unit vector describing the direction on the sphere and T_0 is the average temperature of the CMB. The correlation function of the temperature fluctuations is then

$$C(\theta) = \langle \mathcal{T}(\mathbf{n}) \mathcal{T}(\mathbf{n}') \rangle \tag{8.35}$$

where the average extends over all pairs of directions $\mathbf{n}$ and $\mathbf{n}'$, with angular separation θ.
The power spectrum of temperature fluctuations is usually written as $l(l+1)C_l$ in terms of spherical harmonic order, where the amplitude of fluctuation on an angular scale $\theta \sim \pi/l = 180^{\rm o}/l$. $l = 1$ describes the dipole anisotropy, $l = 2$ the quadrupole, etc.

8.6.3 – The Fluctuation Spectrum

Horizon scale. A characteristic length-scale exists at $z_{\rm rec}$, namely the horizon length. For a flat universe, this is

$$\theta_{\rm H,rec} \approx 1.8^{\rm o} \tag{8.36}$$

Fluctuations on Large Scales. On scales $\gg \theta_{\rm H,rec}$, the Sachs-Wolfe effect dominates since sound waves in the baryon-photon fluid can only occur on scales below the (sound) horizon length. Hence, the CMB angular spectrum

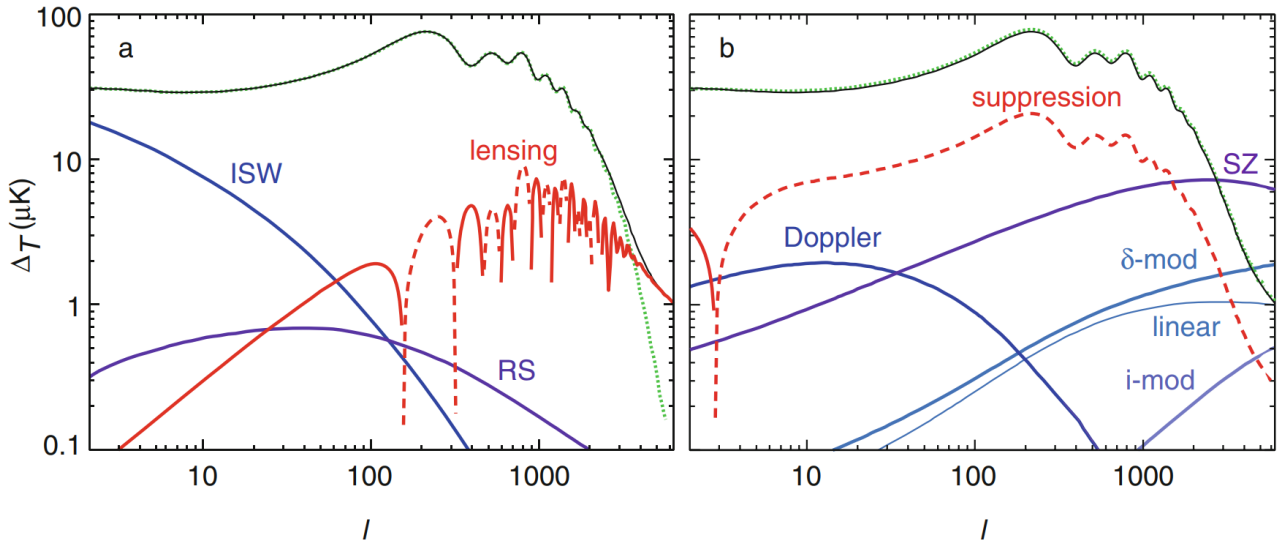

Figure 8.38: The uppermost green curve shows the spectrum of primary temperature fluctuations, whereas the other curves represent the effect of secondary isotropies. Solid curves represent an increase of the temperature fluctuations, dashed curves a decrease. The curve labelled 'suppression' is the scattering by free electrons in the intergalactic medium after reionization, and is the most efficient secondary anisotropy.

reflects the fluctuation spectrum $P(k)$ of matter. In particular, for a Harrizon-Zeldovich spectrum, $P(k) \propto k$, one expects that

$$l(l+1)C_l \approx \text{const.} \quad \text{for} \quad l \ll \frac{180^\circ}{\theta_{\text{H,rec}}} \simeq 100$$

The flat behaviour of the fluctuation spectrum for $n_s = 1$ is modified by the ISW effect.

Silk Damping. Since recombination is not instantaneous but extends over a finite range in redshift, CMB photons are scattered within a shell of finite thickness. Considering a length scale that is smaller than the thickness of this shell, several maxima and minima of T are located within the shell along the line of sight, and so temperature fluctuations on length scales $\lesssim 5'$ ($l \gtrsim 2500$) are greatly damped to yield only very small temperature fluctuations on these scales.

Polarization of the CMB. Although standard blackbody radiation is unpolarised, the CMB is partly polarised. On large angular scales, this is due to CMB photons scattering at low redshifts, i.e. after reionization. We don't expect the scattering during reionization to produce a net polarisation, since it should scatter all in random directions producing no net result. Therefore, the polarization of the CMB at large angles (small l) allows us to measure the scattering optical through the post reionization-era, and thus to estimate the redshift at which the universe became reionized.

8.6.4 – Observations of the CMB Anisotropy

Galactic Foreground. The measured temperature distribution of the microwave radiation is a superposition of the CMB and of emission from galactic and extragalactic sources. Due to its different spectral behaviour, the foreground emission can be identified and subtracted. The galactic foreground basically consists of synchrotron radiation (from relativistic electrons in the galaxy), thermal radiation (by dust), and bremsstrahlung (from hot gas).
To extract the foreground emission from the measured intensity distribution, the microwave radiation can be observed at different frequencies to identify the intensity of each of the aforementioned 3 types of radiation (since they each have different spectral profiles), and subsequently subtracted. As a second way, external data sets may be used.
Besides those galactic foregrounds, extragalactic sources produce emission also – mainly AGN and star-forming galaxies.

8.6.6 – From WMAP to Planck

Gravitational Lensing of the CMB. The prime effect of lensing is that the acoustic peaks and troughs are slightly smoothed out, making them a bit broader and decreasing their amplitude; furthermore, once the primary anisotropies decrease in amplitude due to Silk damping, lensing generates an appreciable power at large l.

Week 9

Ch 8.1 – Redshift Surveys of Galaxies

8.1.1 – Introduction

If it is assumed that the distribution of galaxies traces the underlying distribution of dark matter fairly, the properties of the large scale structure of matter could be studied by observing the galaxy distribution in the universe. Since galaxies have evolved from the general cosmic density field, they should contain information about it.
With photometric sky surveys, the two-dimensional distribution of galaxies on the sphere can be mapped. To also deter-

mine the third spatial coordinate, it is necessary to measure the redshift of the galaxies using spectroscopy, deriving the distance from the Hubble law.

8.1.2 – Redshift Surveys

Recording a spectrum requires much more observing time than determining the apparent magnitude of a source.

The Strategy of Redshift Surveys. Such a survey is basically defined by two criteria. The first is its geometry: a region of the sky is chosen in which the survey is performed. Second, those objects in this region need to be selected for which spectra should be obtained. In most cases, objects are selected according to their brightness for practical reasons (reduces required observing time). For a selection of spectroscopic targets, a photometric catalog of sources is required as a starting point. For instance, a minimum angular extent of objects may be chosen to avoid the inclusion of stars.

Examples of Redshift Surveys. There are a large number of surveys that have observed (collectively) millions of objects in the near to high-redshift universe. The most recent, 2dF and SDSS, also observed QSOs and photometric data, as well as more in-depth spectral data about host galaxies, etc.

8.1.3 – Determination of the Power Spectrum

We now turn to whether or not the distribution of (dark) matter in the universe can be derived from the observed distribution of galaxies. If galaxies trace the distribution of dark matter fairly, the power spectrum or correlation function of dark matter could be determined from the galaxy distribution.

Biasing of Galaxies. We parametrize the connection between dark matter and galaxies by the so-called *linear bias factor* b_g of galaxies. We consider the discrete galaxy field to be smoothed over spheres with radius R, to get the continuous galaxy number density field n, then

$$\delta_g \equiv \frac{\Delta n}{\overline{n}} = b_g \frac{\Delta \rho}{\overline{\rho}} = b_g \delta_R \tag{8.1}$$

where $\Delta n = n - \overline{n}$ is the deviation of the local number density of galaxies from the average density. Hence, the bias factor is the ratio of the relative overdensities of galaxies to dark matter. The galaxy bias factor b may depend on the galaxy type and on redshift, and it also may depend on the smoothing scale R in addition (although for large enough R the density field evolves linearly and we expect this impact to disappear).

Normalization of the Power Spectrum. Analysing spheres of radius $R = 8h^{-1}$ Mpc in the local universe, it is found that optically-selected galaxies have, on this scale, a fluctuation amplitude of order unity:

$$\sigma_{8,g}^2 \equiv \left\langle \left(\frac{\Delta n}{\overline{n}} \right)^2 \right\rangle_g \approx 1 \tag{8.2}$$

where the averaging is performed over different spheres of identical radius R. Accordingly, the dispersion of the matter density contrast is defined as

$$\sigma_8^2 = \left\langle |\delta_{8h^{-1}\mathrm{Mpc}}|^2 \right\rangle \tag{8.3}$$

we then obtain

$$\sigma_8 = \frac{\sigma_{8,g}}{b_g} \approx \frac{1}{b_g} \tag{8.4}$$

Hence if $b_g = 1$, i.e. if galaxies trace the matter distribution fairly, then one has $\sigma_8 \approx 1$. If b_g is not too different from unity, we see that the density fluctuations on a scale of $\sim 8h^{-1}$Mpc are becoming non-linear at the present epoch.

Shape of the Power Spectrum. If we assume that b_g does not depend on the length-scale considered, the *shape* of the dark matter spectrum can be determined from the power spectrum $P_g(k)$ of the galaxies, since $P_g(k) = b_g^2 P(k)$, whereas its amplitude depends on b_g. The shape of $P(k)$ is described by the shape parameter $\Gamma = h\Omega_m$ in the framework of CDM models.

Since a constant b_g can be expected, at best, in the linear domain, i.e. on scales above $\sim 10h^{-1}$Mpc, only such linear scales are used in the comparison with the power spectra predicted by CDM models.

The models which include baryons provide a better fit to the data, with the best fit giving

$$\Gamma = \Omega_m h = 0.18 \pm 0.02, \quad \Omega_b/\Omega_m = 0.17 \pm 0.06 \tag{8.5}$$

8.1.4 – Baryonic Acoustic Oscillations

The length scale of the baryon density perturbation is given by the sound horizon at recombination; it depends only on the baryon-to-photon and matter-to-radiation density ratios. The former is proportional to $\Omega_b h^2$ and the latter is proportional to $\Omega_m h^2$, where one finds that the acoustic scale has a comoving value of $r_s \approx 150$Mpc.

We expect that these frozen sound waves of the baryons leave an imprint on the overall matter correlation function. This unique feature in the correlation function, if it can be detected in the galaxy correlation function, would provide a well-defined 'standard rod' in the observable universe. Since we can observe only angular scales on the sky, the relation between the (comoving) length of the standard rod and the associated angular scale provides a measure of distance. Therefore, a measurement of the baryonic acoustic oscillations in the correlation of galaxies at a given redshift can be used to determine the (comoving) angular diameter distance $f_k(z)$ – which depends only on the density parameters Ω_m and Ω_Λ.

The comoving distance interval corresponding to a redshift interval Δz is given by $\Delta x = c\Delta z/H(z)$. Since there are two transversal dimensions, and one along the line of sight, the distance measured that is determined best from BAOs is the geometric mean

$$D_V(z) = \left(f_k(z) \frac{cz}{H(z)} \right)^{1/3} \tag{8.6}$$

8.1.5 – Effect of Peculiar Velocities

Redshift Space. The relative velocities of galaxies in the universe are not only due to the Hubble expansion, but due to peculiar velocities. The observed redshift of a source is the superposition of the cosmic expansion velocity and its peculiar velocity v along the line of sight,

$$cz = H_0 D + v \tag{8.7}$$

The peculiar velocity therefore causes a distortion of galaxy positions in wedge diagrams, yielding a shift in the radial direction relative to their true positions. Since for most galaxies only the redshift is measurable (and not the true distance D), the observed three-dimensional position of a source is specified by the angular coordinates and the redshift distance

$$s_3 = \frac{cz}{H_0} = D + \frac{v}{H_0} \tag{8.8}$$

The space that is spanned by these three coordinates is called *redshift space*. We expect that the correlation function of galaxies is not isotropic in redshift space (in contrast to our expectation of an isotropic correlation function in real space).

Lecture note: We can measure peculiar velocities statistically (via redshift space distortions), or directly via distance indicators (Cepheids, TRGB, SN Ia, etc).

Galaxy Distribution in Redshift Space. Consider galaxies in a cluster. They are located in a small region in space, thus all at roughly the same distance D and within a small solid angle on the sphere. In real space, they would therefore appear as a three-dimensional galaxy concentration. However, due to the high velocity dispersion, the galaxies span a broad range in s_3, which is easily identified in a wedge diagram as a high stretched structure pointing towards us.

On larger scales, mass concentrations cause the opposite effect: galaxies that are closer to us than the center of this overdensity is then move towards the concentration (due to the gravitational attraction), hence away from us. Therefore their redshift distance s_3 is larger than their true distance D. Conversely, the peculiar velocity of galaxies behind the mass concentration is pointing towards us, so their s_3 is smaller than their true distance. If we now consider galaxies that are located on a spherical shell around this mass concentration, this sphere in physical space becomes an oblate ellipsoid with symmetry axis along the line of sight in redshift space.

Hence the distortion between physical space and redshift space is caused by peculiar velocities which manifest themselves in the transformation (eq 8.8) of the radial coordinate in space. Because of this, the correlation function of galaxies is not isotropic in redshift space.

8.1.6 – Projected Correlation Function

Since the correlation function of galaxies is affected by peculiar velocities, these have to be accounted for if the measured ξ_g (or its equivalent, the power spectrum) is used to determine the power spectrum of the cosmic matter distribution.

Projected Correlation Function. One widely-used method to account for redshift-space distortions in correlation functions is to define the projected correlation function $w_p(r_p)$. It is based on the fact that the peculiar motions affect only the line of sight dependence of the correlation function, whereas the transverse part of it is unchanged. In other words, if $\xi^s(r_p, \pi)$ denotes the correlation function in redshift space, where $r_p = D\Delta\theta = cz\Delta\theta/H_0$ is the transverse separation and $\pi = c\Delta z/H_0$ the line of sight separation, then $\xi^s(r_p, 0) = \xi_g(r_p)$, where $\xi_g(r)$ denotes the isotropic correlation function in physical space. This fact allows us to 'integrate out' the redshift-space distortions by defining

$$w_p(r_p) = \int_{-\infty}^{\infty} \xi^s(r_p, \pi)\ d\pi \tag{8.12}$$

$$= \int_{-\infty}^{\infty} \xi_g\left(\sqrt{r_p^2 + r_3^2}\right)\ dr_3$$

$$= 2\int_{r_p}^{\infty} \frac{r}{\sqrt{r^2 - r_p^2}} \xi_g(r)\ dr \tag{8.13}$$

using the fact that $r^2 = r_p^2 + r_3^2$. If $\xi_g(r)$ is a power law,

$$\xi_g(r) = \left(\frac{r}{r_0}\right)^{-\gamma} \tag{8.14}$$

then $w_p(r_p) = A(\gamma) r_0 (r_p/r_0)^{1-\gamma}$, where the coefficient A depends on the slope. Hence from measuring w_p and fitting a power law to it, one can directly determine the slope γ and the correlation length r_0.

Ch 8.3 – High-Redshift Supernovae and the Cosmological Constant

8.3.1 – Observing SNe Ia at High Redshifts

Supernovae are found through the appearance of a point-like source on the sky, even at high redshift, after subtracting the host galaxy image. To classify SNe as type Ia, a spectroscopic follow up needs to happen (which also determines their redshift).

8.3.2 – Results

The width of the light curve is larger for SNe Ia at higher redshift than it is in the local universe due to a $(1 + z)$ time dilation factor.

Plotting the observed and corrected magnitudes in a Hubble diagram, one can look for the set of cosmological parameters that best describes the dependence of observed magnitudes on redshift. A flat, low matter density model with a cosmological constant fits the data the best.

Comparing the magnitude at the maximum of the measured SNe Ia (or their distance modulus) with that which would be expected for an empty universe, one finds that the SNe are fainter than predicted. In an empty universe, we expect that it would expand at a constant rate (i.e. $\ddot{a} = 0$). Hence we find that the luminosity distance in our universe is

larger than in any other universe with a vanishing cosmological constant. The luminosity distance can only be increased by assuming that the universe expanded more slowly in the past than it does today, hence the the expansion has accelerated over time. It follows that such an expansion is only possible for $\Omega_\Lambda > 0$.
From the highest redshift SNe Ia observed, it was shown that for $z \gtrsim 1$, the trend is reverse and the supernovae become brighter than they would be in an empty universe. At these high redshifts, the matter density dominates the universe, evolving as $(1+z)^3$, in contrast to the constant vacuum energy.

8.3.3 – Discussion

Evolutionary Effects. The above analysis is based on the implicit assumption that, on average, SNe Ia all have the same maximum (corrected) luminosity, independent on their redshift. A z-dependent evolution of SNe Ia, in such a way that they become less luminous with increasing redshift, could have a similar effect on a Hubble diagram as an accelerated expansion. It's been demonstrated that the spectra of high-z SNe Ia are very similar to those of nearby ones, and hence there is no evidence for evolutionary effects. Furthermore, the time until the maximum is reached is independent of z (after accounting for the expansion induced time dilation).
It was a found that host galaxies of higher stellar masses tend to host slightly brighter SN Ia on average. This effect is currently smaller than the statistical uncertainties, and does not affect the conclusions of the cosmological parameters.

Extinction. The correction of luminosity for extinction in the host galaxy and in the Milky Way is determined from reddening. The relation between extinction and reddening depends on the properties of the dust – if these evolve with z, the correct may become systematically wrong. These effects are routinely corrected for using multi-band data, and can be checked by separately investigating SNe Ia that occur in early-type galaxies (in which only little dust exists) and comparing these to events in spiral galaxies.

Lecture Notes

Baryon Acoustic Oscillations. In practice, to calculate separation (distances) in galaxies from a redshift survey, we need to assume a fiducial cosmology. That means we don't directly fit cosmological parameters, as the parameters have some degeneracy in their effect on the observables. Instead, we fit a dilation scale, α, which measures the difference between the true cosmology of the data and our assumed (fiducial) cosmology,

$$\alpha = \frac{D_A(z)^{2/3}\ H_{\rm fid}(z)^{1/3}\ r_{\rm s,\ fid}}{D_{A,\rm fid}(z)^{2/3}\ H_{\rm fid}(z)^{1/3}\ r_{\rm s}}$$

Here, $D_A(z)$ is the angular diameter distance,

$$D_A(z) = \sqrt{\frac{R^2\pi}{\omega}} \tag{4.49}$$
$$= \frac{S_k(r)}{1+z}$$

where R is the source radius covered by a solid angle ω, and r is the comoving distance to the source. $H(z)$ is the Hubble parameter at redshift z, and r_s is the radius of the sound horizon at the baryon drag epoch.

Week 10

Exoplanets

Radial Velocity

Gravity in a system applies to both stars and planets, so planets induce some motion in their stars. This motion means that there is a doppler shift of stellar spectra over the planets orbit, which can then be detected.
A star orbiting its center of mass with a planet in a circular orbit, viewed from within its plane of motion, has a radial velocity with a semi-amplitude

$$K = \left(\frac{2\pi G}{P}\right)^{1/3} \frac{M_p \sin i}{(M_* + M_p)^{2/3}} \frac{1}{(1-e^2)^{1/2}}$$

where i is the inclination of the orbit to the line of sight, and e is the eccentricity of the orbit.
This means RV is sensitive to short periods, large mass planets, high eccentricity, and totally insensitive to face on orbits. Hence, hot jupiters were found first with this method.

Transits

The overwhelming majority of exoplanets have been found via the transit method, where a dip in brightness is found as planets pass in front. Hundreds of thousands of stars can be photometrically monitored in parallel, so it's a very cheap method compared to RV which requires several spectra.

A transit's fractional depth is just the ratio of areas of the planet and star:

$$F = \left(\frac{R_p}{R_*}\right)^2$$

and for a circular orbit, using Kepler's laws the transit duration is

$$t_T \simeq 13 \left(\frac{M_*}{M_\odot}\right)^{-1/2} \left(\frac{a}{1\rm AU}\right) \left(\frac{R_*}{R_\odot}\right) \text{ hours}$$

For randomly oriented planet orbits (like we'd generally expect in the stellar neighbourhood), only around 1% will transit from our perspective, with probability

$$\mathbb{P}(\text{transit}|R_*,\ a) = \frac{R_*}{a}$$

so a transit survey is saturated in efficiency with a perfect telescope.

Direct Imaging

Young planets might be ten thousand times fainter than a star, where older and smaller planets may be on the order of millions or billions. Hence, directly imaging exoplanets is difficult from a contrast perspective.
The imaging of exoplanets is also limited by the diffracted starlight within the telescope optics, where optical errors reduce the sensitivity to exoplanet detection.

Microlensing

As planets (usually rogue planets) pass in front of distant sources (usually distant field stars), the stellar brightness may sharply increase from the gravitational lensing of the planet.

Astrometry

Similar to radial velocity, but looks for a spatial shift in star position rather than the doppler shift in the stellar spectra. The signal amplitude is

$$\alpha = \left(\frac{M_p}{M_*}\right)\left(\frac{a_p}{1\text{AU}}\right)\left(\frac{d}{1\text{pc}}\right) \text{ arcsec}$$

and hence astrometry is sensitive to massive, long period orbits.

Bias

Since each detection method is most sensitive to certain stellar/planetary parameters, there are large swaths of parameter space (planet mass vs period) where no or few detections have been made. In fact, most of the solar system planets are in a poorly sampled region of parameter space.

Transmission Spectroscopy

Transmission spectroscopy involves measuring the spectrum of the star/planet system as the planet transits the star. The spectrum is then sensitive to the absorption of the starlight through the planets atmosphere, which gives an indication of the atmospheric composition. Similarly, emission spectra of the planet can be probed by analysing difference in spectra from when the planet is visible vs when it is obscured by the star in its orbit.

Many of the first exoplanets observed by Hubble had flat spectra in their transit, which is an indicator of clouds or another high albedo property that is relatively independent of wavelength.

Spectroscopy can also be performed directly on the system with direct imaging based off of the reflected light of a planet. Time series spectral lines with this method allows to estimate the orbital parameters of the planet (via the doppler shift in the lines).

Planet Evaporation

Our observational biases mean it is likely to find systems with more massive planets and hot Jupiters. Super-Earths and mini-Neptunes seem to be the most common type of planet found so far. Notably, we see a 'radius gap' in the discovered exoplanets, separating low radius planets ($R \lesssim 1.8R_\oplus$) and higher radius planets ($R \gtrsim 1.8R_\oplus$).
A possible explanation of this is the evaporation of hot Jupiters close to their stars, where their atmosphere and outer layers have been (or are being) stripped away from solar radiation and wind. This evaporation has been observed in flux dip lags around transits as the stripped gasses continue to block starlight after the planet has finished its transit.

Astrobiology

Habitable Zones

Earth is within a 'Goldilocks zone' of temperature that allows liquid water. The distance of this zone away from the star is roughly linear in a stellar mass vs distance from star log-log plot, and so the habitable zone is much closer to the star for lower mass stars. Inside this limit we get runaway greenhouse effects and high temperatures, outside we get ice worlds.
The equilibrium temperature of a planet with albedo A, D distance away from the star of temperature T_* and radius R_* is

$$T_p = T_*(1-A)^{1/4}\sqrt{\frac{R_*}{2D}}$$

The presence of an atmosphere invokes a greenhouse effect – a 'blanket' that radiates equally to space and downwards to the planets surface – that makes the surface of the planet $2^{1/4}$ times hotter for each 'layer' of this blanket.

M Dwarfs

The habitable zone around M dwarfs is small, but surveys show the majority of M dwarfs have planets on short periods. M dwarfs are favoured by the initial mass function, live for many billions of years, and M dwarf planetary transits are deep and frequent.

Red Sky Paradox. If M dwarf planets are so common, why didn't we evolve around an M dwarf? M dwarfs, while cool in median temperature, are very active and have flares, magnetic interactions with the (close) planets and intense bursts of UV radiation.

Galactic Habitable Zone

In the core of galaxies, and very early on, there are many SNe which are not friendly for life. Very far out, and early on, planet occurrence rate might be lower on account of a lower metallicity which is needed for rocky planets with life. The Sun may just have formed at a galactic habitable zone sweet spot!

Life

NASA defines life as being a self-sustaining chemical system and capable of Darwinian evolution.

Venus, the Earth, and Mars were probably formed with similar compositions. Venus underwent a runaway greenhouse effect resulting in the high temperatures we see today. Mars lost its atmosphere from the Solar wind and froze.

Life may have travelled between planets within ejecta after large collisions on planets, the so called 'panspermia'.

Looking for life on other planets (and exoplanets) involves looking for certain biosignatures, namely disequilibrium chemistry – the presence of volatile molecules that would not be present within atmospheres unless continuously replenished by some mechanism (perhaps life) on the planets surface. A notable claimed biosignature is Phosphine on Venus.

SETI

The Drake Equation is a Fermi estimate of the number of civilisations that exist within the Milky Way with which humans could communicate, N, and is given by

$$N = R_* \cdot f_p \cdot n_e \cdot f_l \cdot f_i \cdot f_c \cdot L$$

where [unitless unless said otherwise] R_* is the rate of star formation (units of per year), f_p is the fraction of stars that have planets, n_e the mean number of planets that could support life per star system with planets, f_l the fraction of life supporting planets that could develop life, f_i the fraction of planets with life where life develops intelligence, f_c the fraction of intelligent civilizations that develop communication (or transmit electromagnetic radiation), and L is the mean length of time that civilizations could communicate (units of years).

The Fermi paradox asks why we haven't encountered extraterrestrials in *our* Solar System if they are common in the Universe.

Week 11

Ch 9.1 – Galaxies at High Redshift

9.1.1 – Lyman-Break Galaxies (LBGs)

A breakthrough in discovering galaxies at high redshift is with the *Lyman-break method*. Since hydrogen is so abundant and its ionization cross section so large, photons with $\lambda < 91.2$nm are heavily absorbed by neutral hydrogen in its ground state. Therefore, these photons have a low probability of escaping from a galaxy without being absorbed.
The intergalactic gas absorbs a large fraction of photons emitted by a high-redshift source at $\lambda \lesssim 121.6$nm, and the strength of absorption increases with redshift. Hence, the spectra of high-redshift galaxies should display a distinct break at $\lambda = 91.2(1+z)$nm in the rest frame (for redshifts $\lesssim 4$ and a shift towards $\lambda = 121.6(1+z)$nm for higher redshift galaxies due to the Lyman alpha forest.
Because of this, when we observe in three broadband filters, we should expect light from Lyman-break galaxies to drop out in low-wavelength filters and only being visible at longer wavelengths.

This method of galaxy detection is biased towards those galaxies that have strong UV/blue emission, and hence preferentially selects active star forming galaxies.

The Correlation Function and Halo masses of LBGs. The comoving correlation length of LBGs at redshifts $1.5 \lesssim z \lesssim 3.5$ is not very different from that of L_* galaxies in the present Universe. Since the bias factor of present-day galaxies is about unity, implying that they're clustered in a similar way as the dark matter distribution, this result then implies that the bias of LBGs at high redshift must be considerably larger than unity. This is based on the fact that correlation is based on the squared growth factor of linear perturbations, and so high redshift galaxies having the same correlation means that LBGs are indicators of high-mass dark matter halos. Further, the correlation length increases with the luminosity of the LBG, indicating that more luminous galaxies are hosted by more massive halos.

Proto-clusters. The clustering of LBGs shows that the large-scale galaxy distribution was already in place at high redshifts. In some fields, the observed overdensity in angular position and galaxy redshift is so large that one presumably observed galaxies which will later assemble into a galaxy cluster. Galaxies in such a proto-cluster seem to have about twice the stellar mass of those LBGs outside of the structures, and the age of their stellar population appears older by a factor of two. This indicates that the stellar evolution of galaxies in dense environments proceeds faster than in low-density regions, in accordance with expectations from structure formation.

Winds of Star-Forming Galaxies. There is clear evidence for the presence of massive winds from LBGs. The spectra of LBGs often show strong absorption lines which are blueshifted relative to the velocity of the emission lines in the galaxy. This wind comes from SNe from recently formed massive stars. Characteristic velocities are ~ 200 km/s.

9.1.2 – Photometric Redshift

Spectral Breaks. A stellar population of age $\gtrsim 10^8$ years features a 400nm break because, due to a sudden change in the opacity at this wavelength, the spectra of most stars show a break here. Hence the superposition of billions of stars means that the galaxy of that age will also show such a break, if to a lesser degree.

The Method. When measuring the magnitude of

galaxies in n broad-band filters, we essentially have $n-1$ independent colours. If we have an $(n-1)$ dimensional colour-colour diagram, every galaxy type (no matter its redshift or evolutionary stage) is represented by a unique coordinate. In this idealised consideration, galaxies will occupy a three-dimensional subspace in $(n-1)$ dimensional colourspace parametrised by formation redshift z_f, time-scale τ, and the galaxy's redshift z. Hence from the measurement of the broad-band energy distribution of a galaxy, we might expect to be able to estimate its redshift and the other parameters; this is the method of *photometric redshifts*.

9.1.3 – Other Few-Band Selection Techniques

Narrow-Band Selection. If a source has a strong emission line, and if the observed wavelength of the emission line matches the spectral response of a narrow-band filter, then the ratio of fluxes obtained in this narrow-band image compare to a broad-band image would be much larger than for other sources without a strong emission line at that wavelength.
Candidate images detected in narrow-band images require spectroscopic follow up, since there are many possible contaminants that may enter selection. Galaxies and AGN at lower redshifts can display strong emission lines of other atomic transitions and need to be ruled out of the spectrum.

Ch 9.2 – Deep Views of the Universe

9.2.2 – Hubble Deep Fields

HDFS and the Hubble Ultra Deep Field. One of the immediate results from the Hubble Deep Field was the finding that the morphology of faint galaxies is quite different from those in the nearby Universe. Locally, most luminous galaxies fit into the morphological Hubble sequence. For galaxies at $z \sim 2$, this is no longer true; they are much more compact than local luminous galaxies and show irregular light distributions. By $z \sim 1$ the Hubble sequence is partly established.

Lyman break galaxies at $z \sim 6$ seem to have stellar populations with masses and lifetimes comparable to those at $z \sim 3$. This implies that at a time when the Universe was 1 Gyr old, a stellar population with mass $\sim 3 \times 10^{10} M_\odot$ and age of a few hundred million years (given by the Lyman break) was already in place.
The $z \sim 6$ galaxies are very compact, with half-light radii of ~ 1 kpc.

9.2.3 – Natural Telescopes

The magnification by gravitational lenses can substantially boost the apparent magnitude of source; gravitational lenses can act as natural telescopes. The most prominent examples are the arcs in clusters of galaxies: many of them have a very high redshift and are magnified by a factor $\gtrsim 5$. In addition to boosting the observable fluxes, the gravitational lens also yields a spatial magnification of the source.

The Highest Redshift QSO. The spectrum of the highest redshift QSO (at time of publication) shows a redshift of $z = 7.085$. The luminosity of $\sim 6 \times 10^{13} L_\odot$ implies a very massive black hole with mass $M \sim 2 \times 10^9 M_\odot$ which means that this SMBH mass had to be assembled within the first 800 million years of the Universe, strengthening constraints of rapid black hole formation.

Ch 9.3 – New Types of Galaxies

9.3.1 – Starburst Galaxies

Whereas the Milky Way is forming stars with a rate of $\sim 3 M_\odot$/yr, the star-formation rate in starburst galaxies can be larger by a factor of more than a hundred. Dust heated by hot stars radiates in the FIR, rendering starbursts very strong FIR emitters.
The reason for this strongly enhanced star formation is presumably the interaction with other galaxies or the result of merger processes. During the merger process several massive bursts of star cluster formation are triggered.

The most active regions of star formation are not visible on optical images since they are completely enshrouded by dust; the IR emission is anti-correlated with the optical radiation.
Combining optical, NIR and MIR imaging, starburst galaxies at high redshifts can be detected even if they contain a lot of dust (and thus may fail to satisfy the LBG selection criteria). Studies have found that the comoving number density of starburst galaxies with $L_{IR} \gtrsim 10^{12} L_\odot$ at $z \sim 2$ is about three orders of magnitude larger than the local starburst density. These results imply that the high-ass tail of the local galaxy population with $M \gtrsim 10^{11} M_\odot$ was largely in place at redshift $z \sim 1.5$ and evolves passively from there on.

Ultra-Luminous Compact X-Ray Sources. Observations have shown that starburst galaxies contain a rich population of very luminous compact X-ray sources. They are formally defined to have an X-ray luminosity of $> 10^{39}$ erg/s. Similar sources, though with lower luminosity, are also detected in the Milky Way where these are binary systems with one component being a compact star (WD, NS, or BH). The X-ray emission is hence caused by accretion of matter from a companion star onto the compact component, and are called X-ray binaries.
Some of the ULXs in starbursts are so luminous that the required mass of the compact component far exceeds $1 M_\odot$ if the Eddington luminosity is assumed as an upper limit. Since we don't expect to form BHs with a mass larger than $\sim 10 M_\odot$ in SNe, this implies that these sources are either highly anisotropic (hence beamed towards us) or that the sources are BHs with masses up to $\sim 200 M_\odot$. ULXs are also seen to be concentrated towards the center of galaxies, hence these BHs may spiral into the galaxy's center by dynamical friction and there merge to a SMBH.

9.3.2 – Extremely Red Objects (EROs)

About half of the extremely red objects are found to be elliptical galaxies that already have, at $z \sim 1$, a luminosity similar to that of today's ellipticals, and are at an epoch already dominated by an old stellar population. The other half are galaxies with active star formation which do not show a prominent 400nm break, but which feature the OII emission line (a clear sign of recent star formation). A considerable fraction of EROs are starburst galaxies at $z \sim 1$.

9.3.5 – Lyman-Alpha Blobs

These are luminous and very extended sources of Lyα emission; their typical size is ~ 30 to ~ 100kpc. Some of these sources show no detectable continuum emission in any broadband optical filter.
Suggested explanations are a hidden QSO, strong star formation and its associated superwinds, as well as 'cold accretion' (where gas is accreted onto a dark matter halo and hydrogen is collisionally excited in the gas of temperature $\sim 10^4$K yielding the emission). As a common feature, Lyα blobs are associated with luminous galaxies and are associated with strong infrared emission.

Ch 9.4 – Properties of Galaxies at High Redshift

9.4.1 – Demography of High-Redshift Galaxies

UV-Luminosity Function. The UV-luminosity function of galaxies evolves strongly with redshift. In the redshift interval $2 \lesssim z \lesssim 4$, the characteristic luminosity L^* is about three magnitudes brighter than that of the local UV-luminosity. This shows that a typical galaxy at these redshifts is far more actively forming stars than local galaxies.

Optical/NIR Luminosity Function. The rest-frame optical light is a somewhat better indicator of the total stellar mass of galaxies than is the UV. The results of a combined analysis of optical, NIR and MIR data show a dramatic change of the luminosity function with redshift. The characteristic density of galaxies Φ^* decreases with redshift as one might expect (there should be fewer galaxies around at higher redshifts). For example, at $z \sim 2$, Φ^* is about a factor of 3.5 smaller than the local Universe. In parallel to this, the characteristic luminosity L^* increases with z by about one magnitude up to redshift 2.
It seems that the typical galaxy at high redshift has a larger stellar mass than currently, or that the ratio of high-mass to low-mass galaxies was substantially larger at high z. This implies that with increasing cosmic time, the galaxy population becomes increasingly dominated by those with lower mass. This phenomenon has received the name downsizing.

9.4.2 – The Colour-Magntitude Distribution

The colour bimodality, seen prominently in the local population of galaxies, has been in place at least since $z \sim 2$. At even higher redshift, the sample of galaxies on the red sequence gets increasingly contaminated by dusty star forming galaxies. After correcting for this, the colour bimodality can be detected out to redshifts $z \sim 3$, implying that already at young cosmic epochs were galaxies with old stellar populations coexisting with actively star forming galaxies.
This observed result implies that even at high redshifts, a large fraction of galaxies exist with a passively evolving stellar population. Towards the present time, the red sequence increases in size/decreases compactness.
The local colour-density relation was in place at least since $z \sim 1$.

9.4.3 – The Size and Shape of High-Redshift Galaxies

The Hubble Sequence and Galaxy Morphology. The majority of present day galaxies fall onto the morphological Hubble sequence. The situation at high redshifts is quite different. At $z \gtrsim 3$, most of the galaxies are strongly star forming, with a small population of quiescent galaxies. The star-forming objects do not appear at all to have a regular morphology, rather being irregular or clumpy. Many of them have multiple knot structures, of size ~ 1kpc, which are often separated from the apparent center of the galaxy.

Week 12

Ch 9.6 – The Cosmic Star-Formation History

We define the star-formation rate (SFR) as the mass of the stars that form per unit time in a galaxy, typically given in units of $M_\odot$/yr. Furthermore, we define the star-formation rate density, $\rho_{\rm SFR}$, as that rate per unit (comoving) volume, expressed in $M_\odot {\rm yr}^{-1}{\rm Mpc}^{-3}$.

The Importance of the Initial Mass Function. Since the observable signatures for star formation are obtained only from massive stars, their formation rate needs to be extrapolated to lower masses to obtain the full SFR, by assuming an IMF.

9.6.1 – Indicators of Star Formation

Emission in the Far Infrared (FIR). This is radiation emitted by warm dust which is heated by hot young stars. For this, it is assumed that all the energetic photons from newly born hot stars are absorbed locally and heat the dust; more generally, this expression yields the SFR that is dust enshrouded.

Radio Emission by Galaxies. A very tight correlation exists between the radio luminosity of galaxies and their luminosity in the FIR. Since $L_{\rm FIR}$ is a good indicator of the star formation rate, this should apply for radiation in the radio as well (where we need to disregard the radio emission from a potential AGN component). The synchrotron radio emission of normal galaxies originates mainly from relativistic electrons accelerated in supernova remnants. Since SNRs appear shortly after the beginning of star formation, caused by core-collapse SNe at the end of

life of massive stars in a stellar population, radiation from SNRs is a nearly instantaneous indicator of the SFR.

Hα Emission. This line emission comes mainly from the HII-regions that form around young hot stars with $M \gtrsim 10 M_\odot$. For redshifts $z \gtrsim 2$, the observed Hα lines move into the near IR part of the spectrum and is much more difficult to observe in ground based telescopes.

UV Radiation. This is mainly emitted by O and B stars. This relation sassumes that the UV-flux can leave the galaxy without being attenuated by dust absorption (and neglects that there may be an AGN contribution to the $L_{\rm UV}$). However, in most galaxies this is not a reasonable assumption, and the observed $L_{\rm UV}$ must be corrected for this effect. A typical value for the escape fraction in a Lyman break galaxy is ~ 0.2, which means that the observed UV flux has to be corrected by a factor of ~ 5 to obtain the corresponding SFR.

X-Ray Luminosity. Non-active galaxies are X-Ray emitters. Most of the X-ray emission is due to high-mass X-ray binaries which are members of a young stellar population. About 25% of the X-ray emission from a normal galaxy is due to bremsstrahlung from a hot interstellar medium; since its heating is provided by star-formation activity, it should also scale with the star formation rate.

9.6.2 – Redshift Dependence of the SFR: The Madau Diagram

$\rho_{\rm SFR}$ as a function of redshift specifies how many stars have formed at any time. The plot of this SFR density with respect to redshift is sometimes called the 'Madau' diagram.

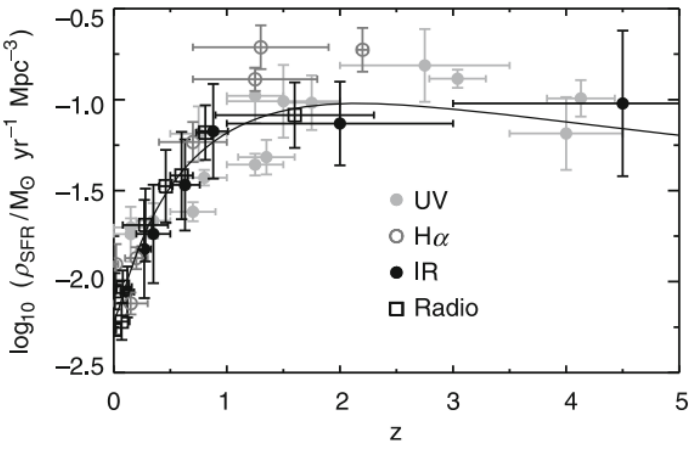

Figure 9.55: Comoving star-formation density $\rho_{\rm SFR}$ as a function of redshift.

There is a strong increase in $\rho_{\rm SFR}$ from the current epoch to $z = 1$ by about a factor 10, a further slight increase towards $z \sim 2$, and a decrease at redshifts beyond that.
Integrating the star-formation density over cosmic time, one obtains the stellar mass density as a function of redshift. From this we conclude that most stars in the present-day universe were already formed at high redshift: star formation at earlier epochs was considerably more active than it is today.
The bottom line is that there was an epoch in the universe, between redshifts $1 \lesssim z \lesssim 4$, where the star-formation activity was the largest. This epohc coincides with the period where the QSO activity was the highest, indicating that the build-up of SMBH mass happened in parallel to the formation of the stellar population.

The Starburst-AGN Connection. In a large fraction of QSOs, clear signs of star-formation activity are found, in some cases at a level where the QSO host galaxy appears as a ULIRG. Conversely, in many of the low-redshift star-forming galaxies, signs of the presence of an AGN are seen. Furthermore, a direct connection between these two processes in a given galaxy does not necessarily have to be observable: it is conceivable that a fresh supply of gas (perhaps from a major merger of galaxies) first leads to a strong star-formation activity, and that the accretion onto the central black hole occurs with some delay – or in reverse order.

Lecture notes. The metallicity at $z \sim 1.5$ is roughly two times lower than the present time, and so high redshift galaxies are less dusty and have a higher gas fraction.
The angular momentum of a galaxy can be expressed in terms of its mass as

$$j_* \propto M_*^\beta$$

where present day galaxies have $\beta \simeq 0.67$, and galaxies at redshifts $z \sim 1.5$-2.5 have $\beta \simeq 0.29$. Hence, galaxies at higher redshift tend to have less angular momentum. A consequence of this relation is that dwarf galaxies had a higher angular momentum (with respect to the present day) relative to more massive galaxies at high redshift.

Ch 2.5.1 – The Gravitational Lensing Effect

Einstein's Deflection Angle. Light, just like massive particles, is deflected in a gravitational field. Quantitatively, it predicts that a light beam which passes a point mass M at a distance ξ (from the point source) is deflected by an angle $\hat{\alpha}$:

$$\hat{\alpha} = \frac{4GM}{c^2 \xi} \tag{2.74}$$

If the deflection is sufficiently strong, light from a very distance source can be visible at two positions in the sky. The Sun is not able to cause multiple images of distance sources, since the maximum deflection angle $\hat{\alpha}_\odot$ is much smaller than the angular radius of the Sun.
The general equation for the angular distance between the true source projection and the lensed image of the source is given by

$$\boldsymbol{\alpha}(\boldsymbol{\theta}) = \frac{4GM}{c^2} \frac{D_{\rm ds}}{D_{\rm s} D_{\rm d}} \frac{\boldsymbol{\theta}}{|\boldsymbol{\theta}|^2}$$

with lens equation

$$\boldsymbol{\beta} = \boldsymbol{\theta} - \theta_E^2 \frac{\boldsymbol{\theta}}{|\boldsymbol{\theta}|^2}$$

Explicit Solution of the Lens Equation for a Point Mass. The Einstein angle of a lens is

$$\theta_E \equiv \sqrt{\frac{4GM}{c^2}\frac{D_{\rm ds}}{D_{\rm s}D_{\rm d}}} \tag{2.82}$$

where $D_{\rm ds} = D_{\rm s} - D_{\rm d}$ is the distance of the source plane from the lens plane, $D_{\rm s}$ is the distance of the source from the observer, and $D_{\rm d}$ is the distance of the deflector from the observer.

Magnification. Light beams are not only deflected as a whole, but they are also subject to differential deflection. For instance, those rays of a light beam that are closer to the lens are deflected more than rays at the other side of the beam. Since gravitational light deflection is not linked to emission or absorption of radiation, the surface brightness (or specific intensity) is preserved. The flux of a source is given as the product of surface brightness and solid angle, and so the observed flux of the source changes since the solid angle subtended by the lensed source is changed (but surface brightness remains constant). If S_0 is the flux of the unlensed source and S the flux of an image of the source, then

$$\mu \equiv \frac{S}{S_0} = \frac{\omega}{\omega_s} \tag{2.85}$$

where ω and ω_s are the observed solid angle of the source and the solid angle the source would subtend if no lens was present respectively.

Ch 3.11.2 – Simple Models

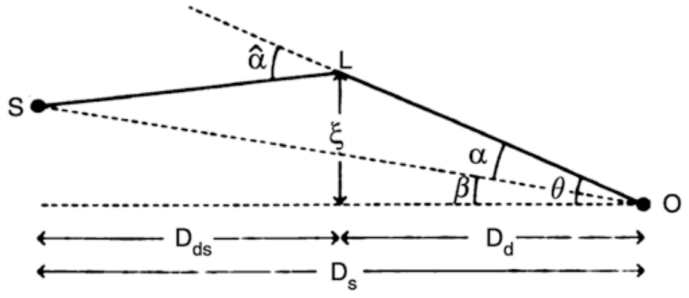

Figure 3.53: Gravitational Lens Geometry. β is the true angular position of the source, that is the angular position at which it would be observed in the absence of light deflection. The position of the light ray in the lens plane is denoted by ξ, and θ is the observed position of the source on the sphere relative to the position of the 'center of the lens' which we have chosen as the origin of the coordinate system $\xi = 0$.

Example: Isothermal Sphere. The rotation curve of the Milky Way, and many other galaxies, is flat for large radii. This indicates the the mass of a galaxy increases proportional to r, thus $\rho(r) \propto r^{-2}$, or more precisely,

$$\rho(r) = \frac{\sigma_v^2}{2\pi G r^2} \tag{3.72}$$

Here, σ_v is the one-dimensional velocity dispersion of stars in the potential of the mass distribution if the distribution of stellar orbits is isotropic. This mass distribution is called a singular isothermal sphere (SIS). This mass model cannot be applied up the the very center of a galaxy since the density diverges for $r \to 0$. Furthermore, the mass diverges up to large r and so the mass profile has to be cut off at some radius in order to get a finite total mass.
The SIS is an appropriate simple model for gravitational lenses over a wide range in radii, since it seems to reproduce the basic properties of lens systems quite well. The deflection angle for a SIS is the Einstein angle with characteristic scale

$$\theta_E = 1.15'' \left(\frac{\sigma_v}{200{\rm km/s}}\right)^2 \left(\frac{D_{\rm ds}}{D_{\rm s}}\right) \tag{3.76}$$

Solution of the Lens Equation for the SIS. If $|\beta| < \theta_E$ then two solutions of the lens equation exist (at angular positions θ_A and θ_B w.r.t to the lens position), and the separation of the images is

$$\Delta\theta = \theta_A + \theta_B = 2\theta_E = 2.3'' \left(\frac{\sigma_v}{200{\rm km/s}}\right)^2 \left(\frac{D_{\rm ds}}{D_{\rm s}}\right) \tag{3.79}$$

Thus the angular position of the images does not depend on the position of the source. For massive galaxies acting as lenses, it is of the order of somewhat more than 1 arcsec.
If $\beta > \theta_E$ only one image of the source exists, and the image is located on the same side of the center of the lens as the unlensed source.
If $\theta \approx \theta_E$, the magnification,

$$\mu(\theta) = \frac{|\theta/\theta_E|}{||\theta/\theta_E| - 1|} \tag{3.80}$$

is very large. Such solutions of the lens equation exist for $|\beta| \ll \theta_E$, so that sources close to the center of the source plan may be highly magnified. If $\beta = 0$, the image of the source will be a ring of radius $\theta = \theta_E$, a so-called Einstein ring.

The SIS has a lens equation

$$\beta = \theta - \theta_E \frac{\theta}{|\theta|}$$

Lecture Notes

For an Einstein de Sitter universe, the relationship between distance and source redshift is

$$D_s = \frac{2c}{H_0}\frac{1}{(1+z_s)}\left(1 - \frac{1}{\sqrt{1+z_s}}\right)$$

$$D_{ds} = \frac{2c}{H_0}\frac{1}{(1+z_s)}\left(\frac{1}{\sqrt{1+z_d}} - \frac{1}{\sqrt{1+z_s}}\right)$$

If we take a spectrum of a source and its redshift differs from that found by the above equations, that means that our assumptions are wrong. This could be due to a different curvature (i.e. the Universe is more/less curved than we

assumed with an Einstein de Sitter model), the mass profile of the deflector is too dissimilar from a point source (perhaps it's not smooth and is not axisymmetric, or needs a cored profile), or the galaxy type is different to what we originally expected.

Week 13

Strain:

$$h(t) = \frac{\Delta L(t)}{L}$$

for the some length of the detector arm and its change in length.

Chirp mass:

$$\mathcal{M} = \frac{(m_1 m_2)^{3/5}}{(m_1 + m_2)^{1/5}} = \frac{c^3}{G}\left[\frac{5}{96}\pi^{-8/3} f^{-11/3}\dot{f}\right]$$

for f frequency of the wave and its derivative in time $\dot{f}$.
There are stochastic gravitational waves (big bang, SMBH background), continuous waves (spinning neutron star with a mountain), chirps (compact binary inspirals), and more. Stochastic waves are generally low frequency with high strain; compact binaries are high frequency with low strain.

Gravitational waves are quadropolar, so

$$f_{GW} = 2 f_{BH}$$

i.e. a black hole will have completed its orbit 4 times if we observe 8 gravitational wave cycles.
Recall $\omega = 2\pi f$ and so

$$\omega_{BH} = \frac{2\pi f_{GW}}{2}$$